Development of Practical Systems to Identify Material Surfaces and Dimensions Using Photograph Images for Room Acoustics Parameters

(室内音場評価のための材料同定・幾何性状計測システムに関する研究)

Graduate School of Engineering, Oita University

Doctor's Course

Doctor's Thesis

2012 March

Musli Nizam bin Yahya

I hereby declare that the work in this thesis is my own except for quotations and summaries which have been duly acknowledged

Student : Musli Nizam bin Yahya (v09f2004)

Date : March 2012

Supervisor : Professor Toru Otsuru

In the name of Allah, the Beneficent, the Merciful

Read! In the Name of your Lord, Who has created (all that exists) (1) Has created man from a clot (a piece of thick coagulated blood). (2) Read! And your Lord is the Most Generous, (3) Who has taught (the writing) by the pen, (4) Has taught man that which he knew not (5).

Surah Al-Alaq; verses: 19; words:1-5

Acknowledgment

Firstly, I would like to express my gratitude toward GOD, who gave me chance and strength all the way from time I was born until today. Secondly, my biggest acknowledgment to my beloved wife Thuwaibah binti Mohd Junaid and children Nurul Munawarah binti Musli Nizam, Muhammad Luqmanulhakim bin Musli Nizam and Muhammad Umarulhakim bin Musli Nizam gave a lot of sacrifices during live in Japan and supporting me mentally, physically and spiritually all the time. I love you all so much. Not forgotten to my family and family in law who always pray for me to finish in my study.

Thank you very much to my advisor Professor Toru Otsuru for the continuous support of my Ph.D study and research, for his patience, motivation, enthusiasm, and immense knowledge. His guidance helped me in all the time of research and writing of this thesis. I could not have imagined having a better advisor and mentor for my Ph.D study.

Besides my advisor, I would like to thank to Associate Professor Reiji Tomiku, Dr. Takeshi Okuzono, Dr. Noriko Okamoto, and Dr. Nazli bin Che Din for your advice and guide. Furthermore, not forgotten to all lab members for helping me in conducting experiments. I have learnt many things from you all. My sincere thanks also go to Mr. Thomas James Harran for proofreading my thesis.

A very special gratitude to my employee University Tun Hussein Onn Malaysia (UTHM) who gave the chance to study at Oita University and also to Malaysia Government for scholarships given.

Thank you again and may GOD bless you all.

Musli Nizam bin Yahya, Oita University

Abstract

This study proposes a practical technique to identify surface material and dimensions for simulating room acoustics parameters e.g. reverberation time. The surface materials and dimensions are obtained from System 1 and System 2, each of which uses photographic images. The study on System 1 uses a Gray Level Co-occurrence Matrix (GLCM) and a Feed Forward Neural Network (FFNN) to identify material surfaces. By identifying material surfaces, absorption coefficients of materials are also determined. Six types of material surfaces such as a wall, a door, a floor, a window, a ceiling and a carpet taken from Oita University rooms are employed. They are captured by using an ordinary camera which is a digital single-lens reflex (DSLR) with 50 mm and f 2.8 lens. The total number of images captured are 36 with the proportions of images are as follows; surface wall = 69 images, surface door = 71 images, surface floor = 66 images, surface window = 56 images, surface ceiling = 67 images, and surface carpet = 40 images. Subsequently, all the images are computed in GLCM to obtain four Haralick coefficients; contrast (cont), correlation (corr), angular second moment (ASM) and homogeneity (hom). Haralick's coefficients are referred to as coefficient values in this study are too wide to be processed because of variations of brightness and texture features. To overcome this problem, a limitation for each coefficient value is made $(\bar{x} - \sigma)$ and $(\bar{x} + \sigma)$, respectively, for a low limitation and a high limitation. The limitations of these coefficient values are represented

in FFNN as input neurons and for the output neuron they are type of material surfaces. By identifying the material surfaces, we are able to ascertain the absorption coefficients of surfaces simultaneously. The results indicate that a good correlation coefficient R $\geq$ 0.90 with MSE $\leq$ 0.07 are provided by System 1 to identify material surfaces. System 2 used a Dimension Vision Predictor (DVP) with the author's "ruler methods" to identify the dimensions of objects. With similar camera uses in System 1, two images are necessary to capture one view. The view of the images displays the ruler and objects to be measured. A ruler is used for standardizing the scale of the objects in the images. Subsequently, both images are fed into DVP to identify the object dimensions. The objects that need to be measured are marked with the corresponding points. To measure one dimension, two corresponding points are connected to make a single line. From the line, DVP identifies the dimension. To investigate the repeatability of System 2, examinations are conducted using 100 objects. The results reveal that the System 2 is highly capable of identifying object dimensions with correlation coefficient R $\geq$ 0.90 and MSE $\leq$ 0.07. From the results, System 2 shows that it has the potential to identify object dimensions. A FFNN technique for estimating room reverberation times is developed. 700 samples of reverberation times obtained using Finite Element Analysis (FEA) are used for FFNN learning processes. In addition 35 unseen data are implemented to confirm the capability of FFNN estimation performance. The results indicate FFNN provides high correlation coefficient R $\geq$ 0.90 with MSE $\leq$ 0.0004 s. To investigate the reliability of FFNN, three conditions in an actual room are created. Reverberation time estimation by FFNN is compared with reverberation time by FEA and reverberation time by measurement. From analysis, MSE between reverberation times using measurement with reverberation times using FFNN are more than 0.002 s. On the other hand, MSE between reverberation times using measurement with reverberation times using FEA are more than 0.005 s. A series of measurement in four practical rooms using both systems are conducted to investigate identi-

fication capability are conducted capability of the systems. An examination of System 1 verified a good correlation coefficient R $\geq$ 0.90 with MSE $\leq$ 0.07 s. Meanwhile, System 2 yields a high correlation coefficient R $\geq$ 0.90 with MSE $\leq$ 0.2 s. Finally, reverberation times for four practical rooms were conducted by using FEA with the important parameters obtained from System 1 and System 2. Sufficient agreements were exhibited by comparing the reverberation times obtained by FEA using both Systems (RT_{FEA} system) with reverberation times obtained by FEA using actual absorption coefficients and dimensions (RT_{FEA} actual). They yielded practical results with correlation coefficient R $\geq$ 0.85 with MSE $\leq$ 0.008 s. In conclusion, a practical technique to identify surface materials and dimensions using photographic images yielded practical results. With some improvements such as adding more Haralick coefficients and standardize room illumination, the techniques will be more accurate, effective and practical when applied in the actual rooms. Furthermore, it is useful for simulating room acoustics parameters such as FEA, BEA, Ray tracing and so on.

Contents

List of Figures

List of Tables

Chapter 1.

Introduction

1.1. Background of Study

Absorption coefficients and dimensions of rooms are important parameters that are useful in predicting the room acoustics paramaters (e.g. reverberation time) that are necessary for use with theoritical technique such as Sabine [1], Eyring [2], Millington [3], Fitzroy [4], and Empirical [5] and computational technqiue such as Ray Tracing [6, 7], Finite Element Analysis [8, 9], and Boundary Element Analysis [10, 11].

Generally, absorption coefficients are derived from physical measurements either by using an impendence tube method or a reverberation room method which requires special equipment, skills and more time consumption. Therefore, several reports have proposed new techniques for predicting the absorption coefficient without using physical equipment such as the following;

1. Min et al. [12] used neural network to estimate three different absorption coefficients of perforated wooden panel which are douglas fir (DF), spure fir pine (SFP), and western red cedar (WRC) with different backing layer

namely no backing material, glass fiber backing and nanofiber backing attach on the panel. However, this work focuses only perforated panel.

2. Hodgson and Scherebnyj [13] developed a technique to estimate multi absorption coefficients of eight types of surfaces in classroom for University British Columbia (UBC) from early-decay time and multivariable linear-regression. The eight types of surfaces were; i. hard surfaces, ii. paneled surfaces, iii. glued-on acoustical tiles, iv. suspended acoustical ceiling, v. carpeted surfaces , vi. upholstered seats , vii. porous absorbers , viii. and Helmholtz-resonator absorbers

   This study conducted calculation to obtain absorption coefficients. It was useful for UBC classroom and appropriate for those experts in acoustics fields.

3. A study from Hodgson [5] proposed empirical technique to predict of speech levels and reverberation in classroom. He used multi-variable linear regression technique to develop an equation. The equations used are;

$$EDT1 = 1.4395 + 0.0034LW - 5.05\alpha l + 0.1632refl - 0.1973absdist + 0.2981basic \tag{1.1}$$

$$EDT1 = 0.8744 + 0.00221LW + 0.303refl + 0.4116basic - 0984absorb - 0.8044upseat \tag{1.2}$$

Table 1.1 shows parameters used on his work. Parameters from *refl* to *upseat* are obtained from references or from experience. Thus, this technique is useful for expert in acoustic fields.

Overall, all the studies proposed new techniques to obtain absorption coefficients but it is unsuitable for persons who not expert in acoustics fields.

Table 1.1.: Parameters used in the empirical prediction models, and ranges of values in datasets

Parameter	Description	Unit	Database Range
$L.W$	classroom length x width (i.e floor area)	m^2	36.5 to 484.8
L	classroom length	m	4.4 to 24.0
H	classroom height	m	2.2 to 8.0
fwdist	distance from source to front wall	m	0.44 to 3.2
αl	average surface-absorption at 1kHz	-	0.06 to 0.29
$log\alpha l$	$\log_{10}(\alpha l)$	-	-1.22 to -0.54
refl	Beneficial room shape, reflector?: no=0, yes=1	-	0 and 1
absdist	Benificial absorption distrubition?: no=0, yes=1	-	0 and 1
basic	absence of sound-absorption features?: no=0, yes=1	-	0 and 1
absorp	Extent of absorbent ceiling/wall treatment: full wall or ceiling	-	0.0 to 1.0
upseat	upholstered seating?: no=0, yes=1	-	0 and 1

While, dimensions are obtained from physical measurements such as laser or tape measurements. CAD drawings can produce room dimensions but it remains necessary to take measurements in situations where no drawing is available. Lately, 3D scanner technology is widely used to estimate room dimensions [14, 15, 16]. Although such scanners provide precise measurements, they are expensive and require long post processing.

To identify parameters of rooms, two simple systems using photographic images are proposed in this work. Three techniques are used to build the systems: i. a Gray Level Co-occurrence Matrix (GLCM); ii. a Dimension Vision Predictor (DVP); and iii. a Feed-Forward Neural Network (FFNN). These techniques yield two systems. System 1 uses GLCM and FFNN to identify room material surfaces. By identifying such materials, corresponding absorption coefficients are also given. System 2 uses DVP to identify room dimensions.

The accuracy of the two systems is examined by using actual rooms to investigate the identification capability of the two systems. The absorption coefficients and dimension identification from the two systems are used to compute reverberation times of actual rooms.

As known, reverberation times is one of the important acoustics pa-

rameters for rooms. It is recommended that the reverberation time, especially classroom should be less than 0.6 s and 0.7 s for 200 $m^3$and 300 m^3respectively, at one-octave-band-pass-filtered impulse responses average between 500 Hz and 1 kHz. [17]. In general, three factors affect the reverberation time values; volume, proportion (shape) and absorption coefficient of mterial surface. Practically, measuring technique using ISO 3382 [18] is commonly used to obtain the reverberation times because it offer accurate results. However, it is impossible to measure a room in under construction or nonexisted (on paper design). Theoretical technique such as Sabine and Eyring can be used but it is compromised for non-diffuse and non-uniform surface absorption coefficient surroundings. Many researchers have proposed new methods which are computational technique such as Ray-Tracing, Finite Element Analysis and Boundary Elopement Analysis such as to surpass those kinds of lacking on the Sabine and Eyring [19, 20, 21]. Nevertheless, Ray-Tracing, Finite Element Analysis and Boundary Element Analysis typically require more times to analyze. In this study we used FFNN because it is able to give the less time of analysis and has friendly user interface.

To develop FFNN, training databases are essential. To achieve that, FEA is used to simulate reverberation time's database FFNN training process. The FEA was chosen because of high accuracy, especially in the lower frequencies (125 kHz to 1 kHz) regions. After the development of FFNN is completed, it will be used for estimating the reverberation times at actual rooms. FFNN needs parameters to estimate the reverberation times. Therefore, the estimation parameters from System 1 and System 2 are used. Subsequently, the estimation reverberation times from FFNN are compared FEA with both using same absorption coefficients, and dimension obtained from System 1 and System 2.

1.2. Objectives

The objectives of this study are;

1. To propose a practical systems for estimating the material surfaces and dimensions of room that can be used for simulating room sound field,

2. To develop Feed Forward Neural Network to estimate the reverberation times of room, and

3. To compare the reliability between Feed Forwad Neural Network and Finite Element Analysis in estimating reverberation times of room using parameter from practical systems .

1.3. Scopes

The scopes that are set to achieve the main objectives are listed as follows:

1. Oita University rooms were selected as the scope of the study. They were used for collecting database to develop systems and were also used for investigating the capability of systems at actual rooms.

2. Only six material surfaces were employed in this study in order to establish the concept of estimating material surface.

3. Two computational techniques FFNN and FEA were used to simulate the reverberation times of rooms.

1.4. Significant of the Study

Generally, to identify an absorption coefficient, conducting physical measurements are necessary. To perform such measurements, it is necessary to use special equipment and to follow complicated procedures, which are time consuming, and expensive. The measurement only can be conductud by an expert in the acoustic field. Similar problems are also occurred at room dimensions identifying if the objects are difficult to measure i.e. objects is located at a high place. To surmount both problems, the author develops systems that capable to estimate absorption coefficients and dimension of objects using photographic images. By using these systems, we can ascertain room parameters in a room field easily, rapidly, and at a low cost. It is also useful, especially when an expert on acoustics in not available. By System 1 and System 2 estimations, the acoustic fields of room i.e reverberation times able to simulate using approximate techniques (theoretical or computational).

1.5. Outcome of the Study

As an outcome, it is expected that the System 1 will be able to identify the room material surfaces. Simultaneously, we are also capable of ascertaining the room absorption coefficients. To identify the material surfaces, this system gave results in classification numbers from 1 to 5, which each number represents the material surface. From that number, then we can identify the types of material surfaces and absorption coefficients.

Meanwhile, it is expected that System 2 will be able to identify the dimension of any objects. However, for room acoustical, the room dimensions are the objects that supposed to be identify.

By using both systems, it can be used to simulate the actual rooms' reverberation times whether using theoretical techniques and computational techniques. For investigating the capability for estimating the actual room parameters, in this study FFNN and FEA are adopted for simulating the rooms' reverberation times. Then, the results from FFNN and FEA are compared.

1.6. Limitations of the Study

The limitations of this study are as followS;

1. It can only identify the material surfaces depending on the database of material surfaces used. If more databases of material surfaces were used, then more material surfaces can be identified.

2. Generally, the real absorption coefficients of material surfaces in rooms depend on the material thickness, presence or absence of an air layer and absorptive layer, and so on. Therefore, it is difficult to obtain a real absorption coefficients from only a surface form image. For practical usage, the author refers to related reports of the absorption coefficient.

3. Training database of reverberation times obtained from FEA is used for FFNN training process. To simulate training database of reverberation time using FEA, this study uses only eight rooms with difference volumes. In simulation, six absorption coefficients of material surface of wall, door, floor, window, ceiling and furniture are considered. Generally, absorption coefficient's values are 0 to 1, which depending on the type of material either reflective of absorptive. To consider all values, it will increase the computing time and cost on FEA. Thus, the author only uses two conditions; dead and live which respectively presents the maximum values and minimum values of the absorption coefficient for each material surface.

1.7. Flow of the Systems

There are two kinds of systems that brings significance to the research; System 1 and System 2. As mentioned before, System 1 is used to identify the material surfaces at the same time absorption coefficients are obtained. Meanwhile, System 2 is used to identify room dimensions. As a result, these systems can be implemented after their developments are completed. The results from System 1 and System 2 can be used in theoritical technqiue or computational techniqie. Here, FFNN and FEA are used to estimate the reverberation times of room using parameters obtained from System 1 and System 2. The FFNN and FEA results are compared to investigate the reliability in estimating reverberation times. Detail explanations of each step of methodology are shown in Fig 1.1.

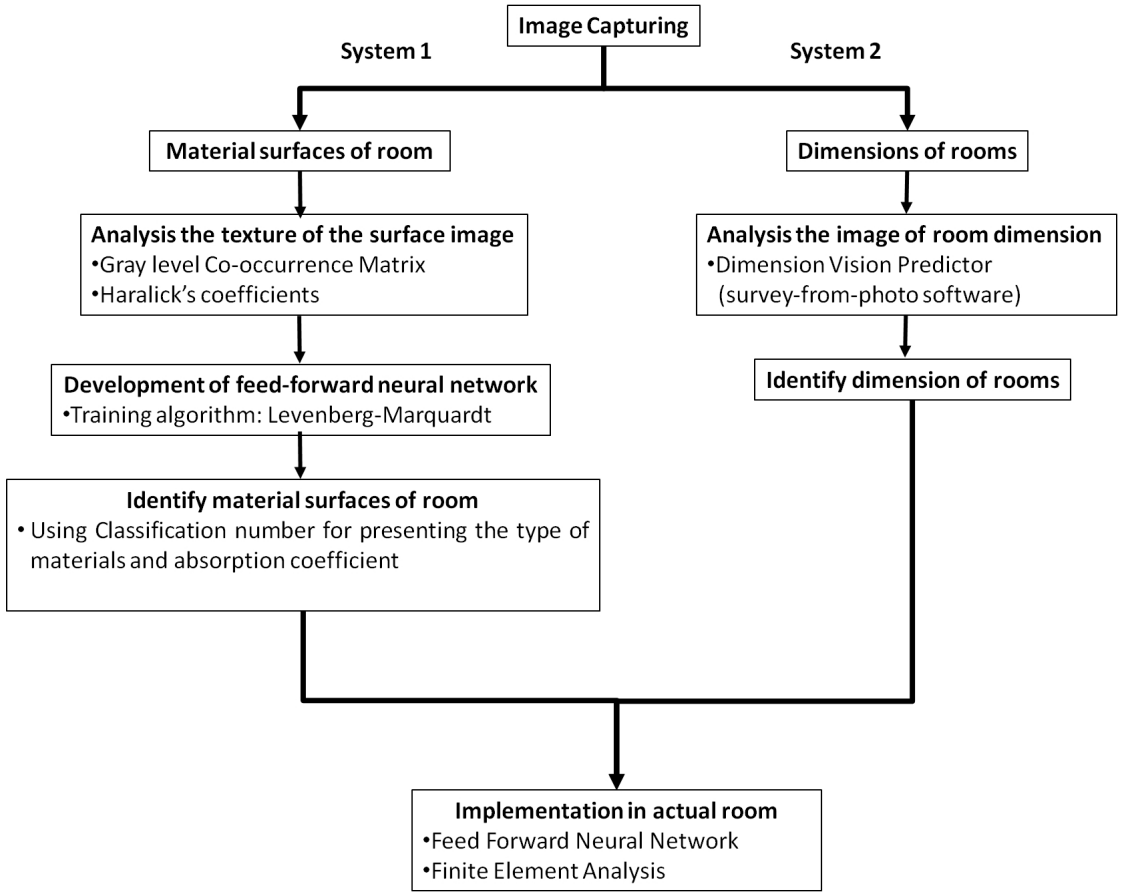

Figure 1.1.: The flow of the System 1 and System 2

Chapter 2.

Theoretical Descriptions

2.1. Introduction

This chapter discusses GLCM, DVP, and FFNN which are the techniques used in this study. Furthermore, the FEA is also discussed in this chapter which is used to simulate the room reverberation times.

2.2. Absorption Coefficient

Absorption coefficient is a fraction of incident sound intensity, which is either absorbed or transmitted. Absorption coefficient is useful when using theoretical or computation technique to evaluate the growth and decay of sound energy in the room. The value of an absorption coefficient is depended on the type of sound incident on the material surfaces, i.e. normal incidence, oblique incidence and random incidence as shown in Figure 2.1. Normal incidence is when the sound incident angle is 0^o, while, oblique incident is when the sound incident angle to be at a certain angle, and random incidence is when the sound incidence

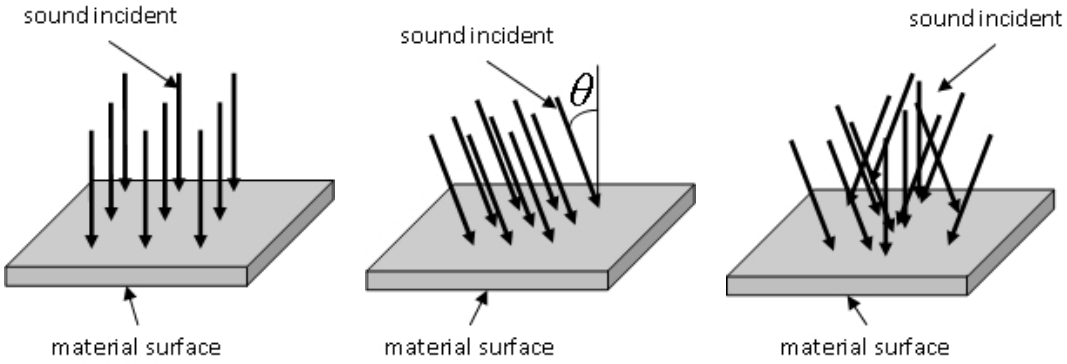

(a) normal incidence (b) oblique incidence (c) random incidence

Figure 2.1.: Type of Sound Incidence

to be at all angles. These incidences can be expressed as follows [22],

$$\alpha = 1 - (rp)^2 = 1 - \left(\frac{n-1}{n+1}\right)^2 \tag{2.1}$$

$$\alpha_\theta = \frac{4r_n cos\theta}{(r_n cos\theta + 1)^2 + (x_n cos\theta)^2} \tag{2.2}$$

$$\alpha_s = \frac{\int_0^{\frac{\pi}{2}} \alpha_\theta sin\theta cos\theta d\theta}{\int_0^{\frac{\pi}{2}} sin\theta cos\theta d\theta} = \int_0^{\frac{\pi}{2}} \alpha_\theta sin\,(2\theta)\, d\theta \tag{2.3}$$

Generally, the value of absorption coefficients is given between 0 and 1, where 1 is a perfect absorption, and 0 is a perfect reflector.

2.3. Reverberation times

Reverberation is phenomena occur when the sound source stop, the sound energy still be heard for some time until sound energy decays away to inaudibility . To compute reverberation mathematically, the reverberation time is defined as the time required for the average sound energy density to decay by 60

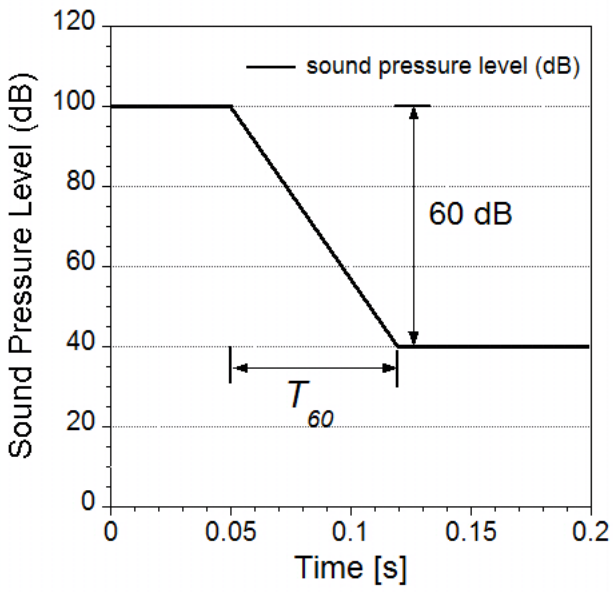

Figure 2.2.: Example sound pressure level in a room decays in time

dB after the sound source is stopped as illustrated in Figure 2.2. Sabine [1] who studied the phenomena was proposed equation to compute reverberation time. Reverberation time has been used as an important indicator of room acoustic characteristic or auditory environment of room.

$$T_{60}[s] = \frac{0.161V}{A} \tag{2.4}$$

$$A[\mathrm{m}^2] = \sum S\alpha \tag{2.5}$$

where V (m^3) is volume of the room, A (m^2) is the total absorption coefficients, S is total surface area in side the room, and α is average absortiom coefficient.

2.4. Gray Level Co-occurrence Matrix (GLCM)

2.4.1. Introduction of Image Texture

The texture feature is defined as a function of the spatial variation in pixel intensity [23]. The Image texture is one of the important characteristics in identifying objects or regions of interest in an image [24]. It is contained of information of size, shape, color and orientation of the elements of the pattern. The differences between two image textures are depending on the information. Base on that information, many techniques can be applied such as multiplicative auto regressive random fields, fourier transforms of the cosine transforms, fractal dimension, wavelet-based Information, ridgelet-based Infromation, and so on to obtain the analysis of the texture features.

2.4.2. Theory of Gray Level Co-Occurrence Matrix (GLCM)

Recently, there are numerous approaches available such as multiplicative auto regressive random fields, fourier transforms of the cosine transforms, fractal dimension, wavelet-Based Information, ridgelet-Based Infromation, and so on to analyze the texture features. Although, such techniques provide different advantages in terms of capability analysis texture features, GLCM is the best approach in terms of its higher texture analysis accuracy. [25].

GLCM is one of the texture feature analysis which can compute the texture features of image by second order statistical approach [26]. It has been successfully implemented to analyze the texture features in many fields [27, 28, 29, 30, 31]. To date, no reported study has applied GLCM for acoustic fields.

A GLCM is generated from a square matrix (Ng) with size is determined according to the gray levels of pixels of an image that can be captured using a

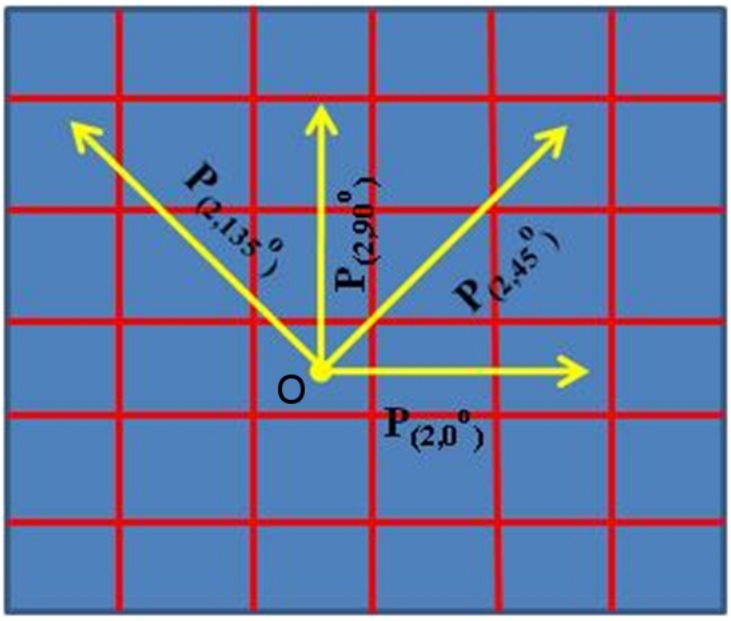

Figure 2.3.: Example of directions between two image pixels ($d = 0$; $\theta = 0^o, 45^o, 90^o, 135^o$)

digital camera. An image includes numerous pixels, each of which presents a level of gray. A square matrix Ng is formed at these pixels.

A GLCM comprises numerous elements, each designated as probability $P_{d,\theta}(i,j)$. The $P_{d,\theta}(i,j)$ represents pixels with gray levels i and j, which are counted at certain distance d (e.g. $d = 1$ or 2) and direction angle θ ($\theta = 0°$, 45°, 90° and 135°) between the two image pixels. Basically, in one image will provide four GLCMs depending on the d and θ. Figure 2.3 illustrates an example of direction (d and θ) for computing GLCMs. **O** is indicated the corresponding origion of pixel.

For a detailed explanation, Fig. 2.4 present examples of an gray level image pixel with the range is between 0 to 4. As mentioned before, four direction angles are implemented to calculate GLCMs at an image, Figure 2.5 to 2.8 show examples to calculate the GLCMs. Referring to the Fig 2.5, the size of GLCM is depended on the range of the grey level at the image. The size of i and j is from 0 to 4. To calculate the GLCM with $d = 1$ and $\theta = 0°$, firstly, we refer to the i and j value. In this example the i and j is 4 and 2 respectively. Secondly, we

Figure 2.4.: Gray level of an image

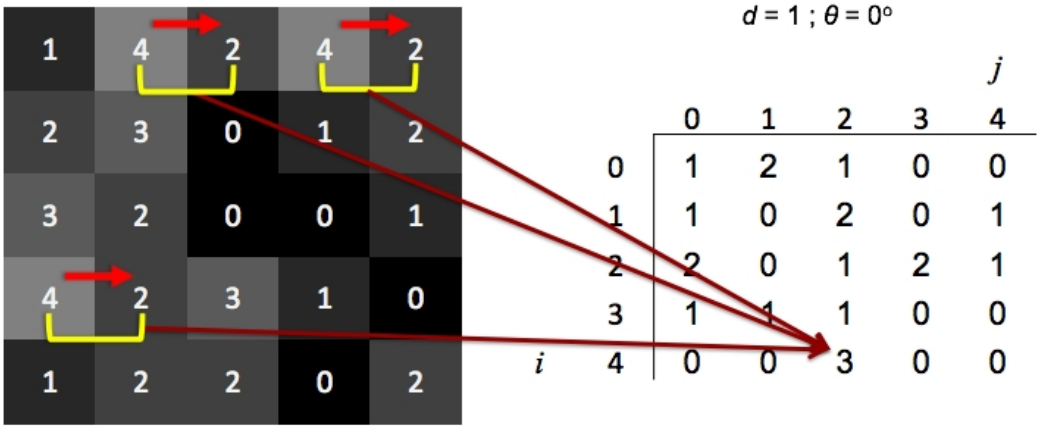

Figure 2.5.: GLCM for $d = 1$ and $\theta = 0°$

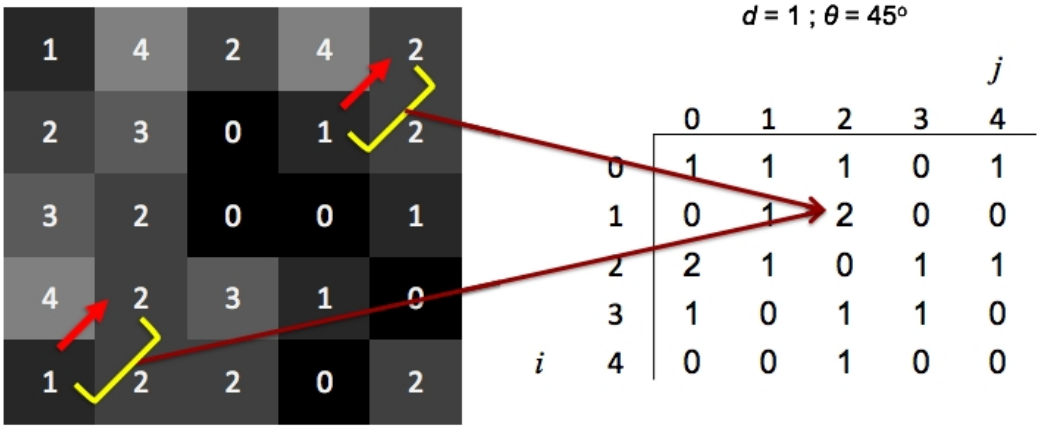

Figure 2.6.: GLCM for d = 1 and $\theta = 45°$

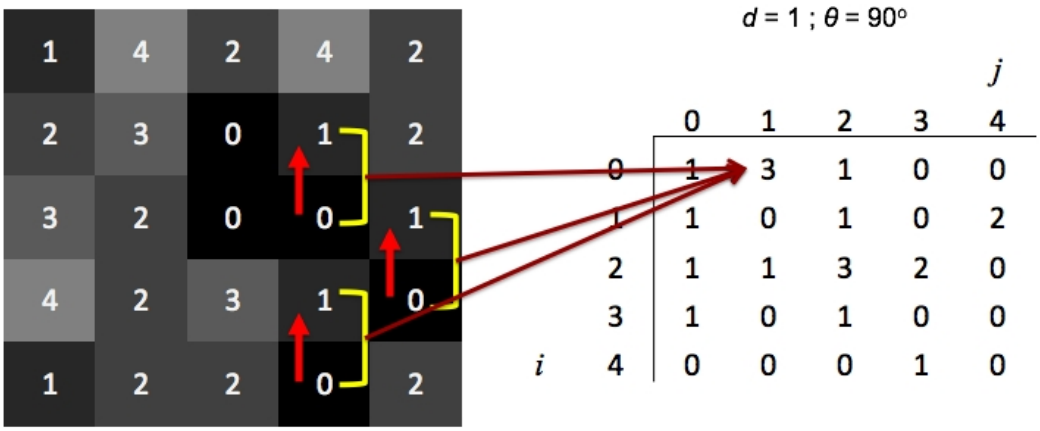

Figure 2.7.: GLCM for $d = 1$ and $\theta = 90°$

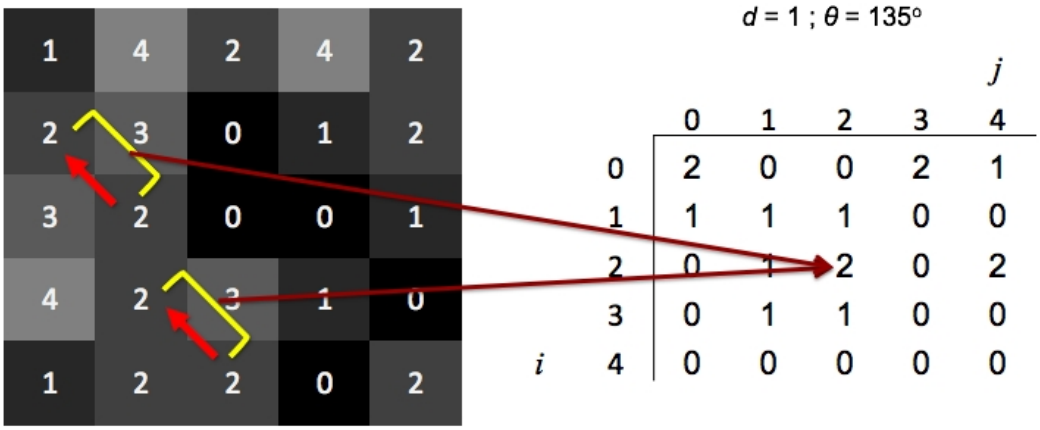

Figure 2.8.: GLCM for $d = 1$ and $\theta = 135°$

refer to the image and find the partner of two image pixel based on the i and j value with the distance $d = 1$ and direction angle θ= 0°. Subsequently, we count the frequency of i and j value. The result reveals that the intensity of $i = 4$ and $j = 2$ is 3. Following such procedure, a GLCM can be obtained.

A similar process is conducted for $d = 1$; $\theta = 45°$, d =1; $\theta = 90°$ and $d = 1$; $\theta = 135°$ as shown in Fig. 2.6, 2.7, and 2.8, respectively. To count the intensity of i and j, the directions are referred to d and θ. Figure 2.6 portrays an example to count the intensity of $i = 1$ and $j = 2$. By referring the $d = 1$ and θ = 45°, the intensity of i and j is 2. Moreover, 2.7 and Fig. 2.8 show an example to count the intensity of $i = 0$ and $j = 1$, and $i = 0$ and $j = 1$, respectively. By referring to the d and θ, the respectivelyintensity for $i = 0$ and $j = 1$, and $i = 0$ and $j = 1$, is 3 and 2.

Generally, GLCM is difficult to implement directly if the computing procedure involves wide gray scale level. Therefore, Haralick [32] proposed 14 coefficient of texture features . The four commonly used Haralick coefficients are listed below as follow[30, 31];

$$cont = \sum_{i=0}^{Ng-1} \sum_{i=0}^{Ng-1} P_{d,\theta}(i,j) \cdot (i-j)^2 \tag{2.6}$$

$$corr = \frac{\left\{\sum_{i=0}^{Ng-1} \sum_{j=0}^{Ng-1} P_{d,\theta}(i,j) \cdot (i,j)\right\} - \mu_x \mu_y}{\sigma_x \sigma_y} \tag{2.7}$$

$$ASM = \sum_{i=0}^{Ng-1} \sum_{j=0}^{Ng-1} \{P_{d,\theta}(i,j)\}^2 \tag{2.8}$$

$$hom = \sum_{i=0}^{Ng-1} \sum_{j=0}^{Ng-1} \frac{P_{d,\theta}(i,j)}{1+(i-j)^2} \tag{2.9}$$

In the above equations, *cont* is the contrast used to measure the image contrast, *corr* is the correlation used to measure image linearity, and ASM is the angular second moment used to measure image smoothness or some called Energy. *hom* represents the homogeneity used to indicate homogeneity in uniform images. In addition, μ_x, μ_y, σ_x, and σ_y are the respectively means and standard deviations of GLCM are expressed below [30] ;

$$\mu_x = \sum_{i=1}^{Ng-1} i \sum_{j=1}^{Ng-1} P_{d,\theta}(i,j) \tag{2.10}$$

$$\mu_y = \sum_{j=1}^{Ng-1} j \sum_{i=1}^{Ng-1} P_{d,\theta}(i,j) \tag{2.11}$$

$$\sigma_x = \sum_{i=1}^{Ng-1} (i-\mu_x)^2 \sum_{j=1}^{Ng-1} P_{d,\theta}(i,j) \tag{2.12}$$

$$\sigma_y = \sum_{j=1}^{Ng-1} (j-\mu_y)^2 \sum_{i=1}^{Ng-1} P_{d,\theta}(i,j) \tag{2.13}$$

2.5. Feed-Forward Neural Network (FFNN)

2.5.1. Analogy of Human Brain

In recent years FFNN has become a popular method of solution in various disciplines. These include engineering, business, and defense. FFNN was created from non-linear computational elements operating in parallel and close interconnection. The concept of FFNN was inspired from the biological human

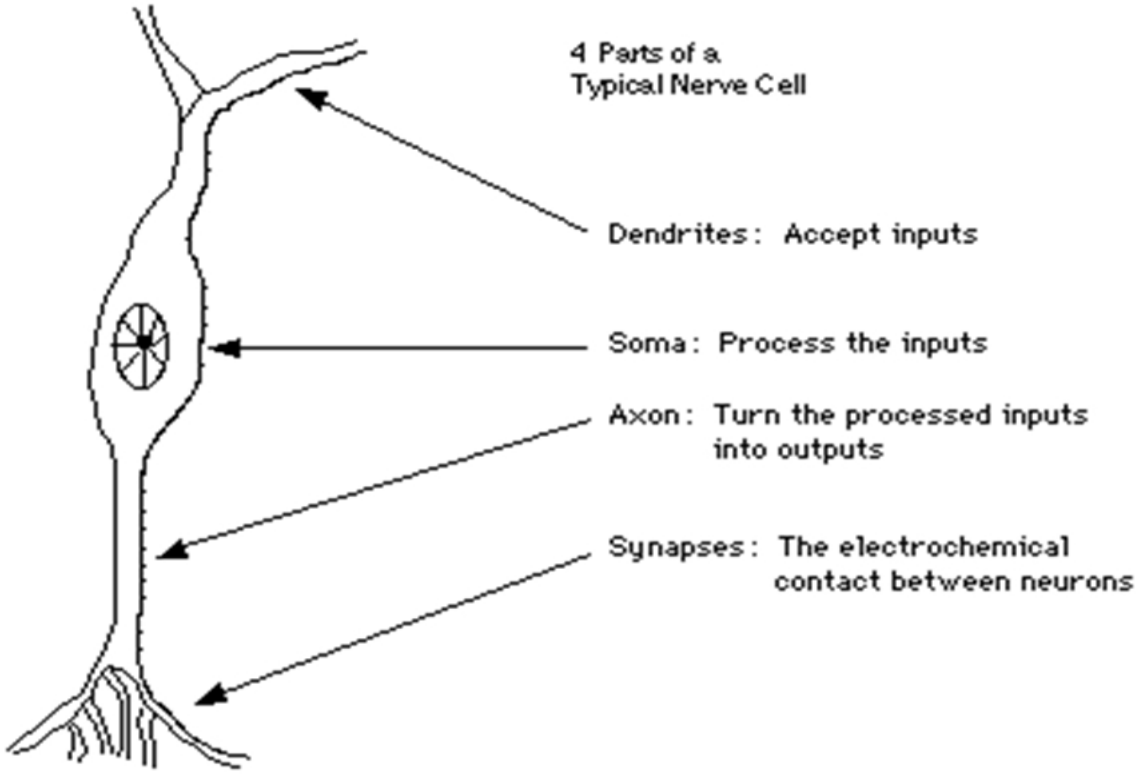

Figure 2.9.: Human nerve cell

brain structure called nerve cell as illustrated in Fig. 2.9 . The FFNN consists of neurons, which are regarded as similar to a nerve cell. Each neuron is interconnected among them to become a structure of neuron's connections, which is called the architecture of FFNN. Each of the connections consists of a weight and bias, which can be adjusted during the training phase. The FFNN stores all the knowledge in the connections between neurons and extracts them. Such knowledge is able to recall using some elements, which are called input parameters. By this information, the FFNN is able to recognize new input parameters even though they never have been presented before [33]. Explainations of architecture of FFNN is given in next topic.

FFNN is being applied to an increasing number of real-world problems of considerable complexity. The advantages of FFNN are [34, 35];

1. Learning : FFNN is able to adapt without assistance of the user. It is learning from the historic process of database (input - output).

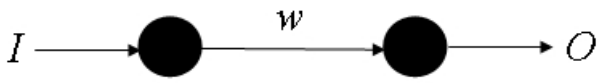

Figure 2.10.: Single input neuron

2. Non-linearity: A neuron is non-linear device. Consequently, FFNN is a non-linear. It is making no assumptions about input distributions and uses non-linear neurons functions.

3. Robustness: FFNN are very robust. Their performance degrades gracefully in the presence of increasing amounts of noise.

4. Generalization: A properly trained model possesses generalization ability due to which it can be accurately predict outputs for a new input data set and even multi-output relationships can be simultaneously approximated.

2.5.2. Basic Element of Neural Network

2.5.2.1. Single Input Neuron

Single Input Neuron is a system that receives one input data and generates only one output data. Figure 2.10 shows that neuron has one input I. I is multiplied by weight w, to form wI and sent to the summer $\sum$. Another input of 1 is multiplied by bias θ and went through to summer. The summer output n is a net input that goes through to transfer function f, which produces the scale neuron output O. The neuron output is calculated as (Haqan et.al., 1996):

$$O = f\left(wI + \theta\right) \tag{2.14}$$

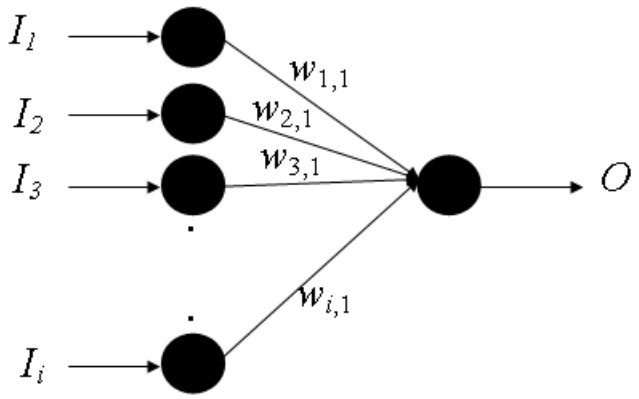

Figure 2.11.: Multi input neuron

2.5.2.2. Multiple Input Neuron

Multiple input neuron is a system which is able to receive more than one inputs. Figure 2.11 shows the structure of multiple input neurons with the inputs I_1, I_2, $I_3 \ldots I_i$ which are able to generate one output. Each input has its own corresponding weight, which is defined by $w_{1,1}$, $w_{2,1}$, $w_{3,1}$, . . . $w_{i,1}$ of the weight matrix **W**. In this system, bias θ, the summer, adds all the weight inputs to form the net input n:

$$n = w_{1,1}I_1 + w_{2,1}I_2 + w_{3,1}I_3 + \ldots + w_{i,1}I_i + \theta \tag{2.15}$$

In matrix form:

$$n = \mathbf{WI} + \theta \tag{2.16}$$

Where **W** is the weight matrix.

The neuron output can be written as:

$$O = f\left(\mathbf{WI} + \theta\right) \tag{2.17}$$

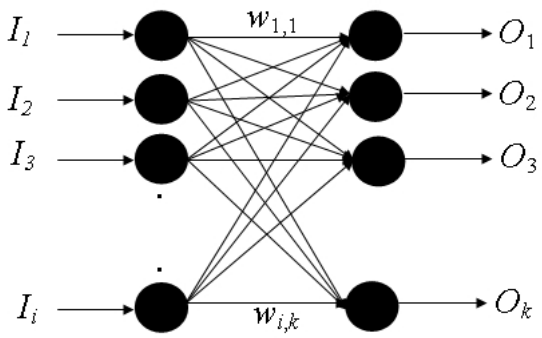

Figure 2.12.: Single layer

2.5.2.3. Neurons Layer

Neural network architecture is formed when the neurons of a network are intimately linked with the learning algorithm to train the network [33] . Commonly, one neuron with many inputs may not be sufficient. Thus, it might need more than one operation in parallel to provide the sufficient network that is called layer [36]. Each layer contains a certain number of units or some called nodes where each unit receives input signals directly from the previous layer and sends output signals directly to units in the next layer. Generally, there are two different classes of neural network architectures; single layer neuron and multiple layers neuron.

- Single Layer

Single layer neuron is the simplest form of a layer network that consists of input layer of source nodes and output layer of computational nodes . The input nodes are directed through the output layer without any connection of other layer. Figure 2.12 shows the single layer neuron where each element of the vector I_i is an input that is connected to each neuron through the weight matrix $W_{i,k}$. the input signal, weighting and bias θ are summed to generate the net inputs O_k. This is a simple network compared to multiple layers neuron that have one or more layers among the input and output signal which is called hidden layers.

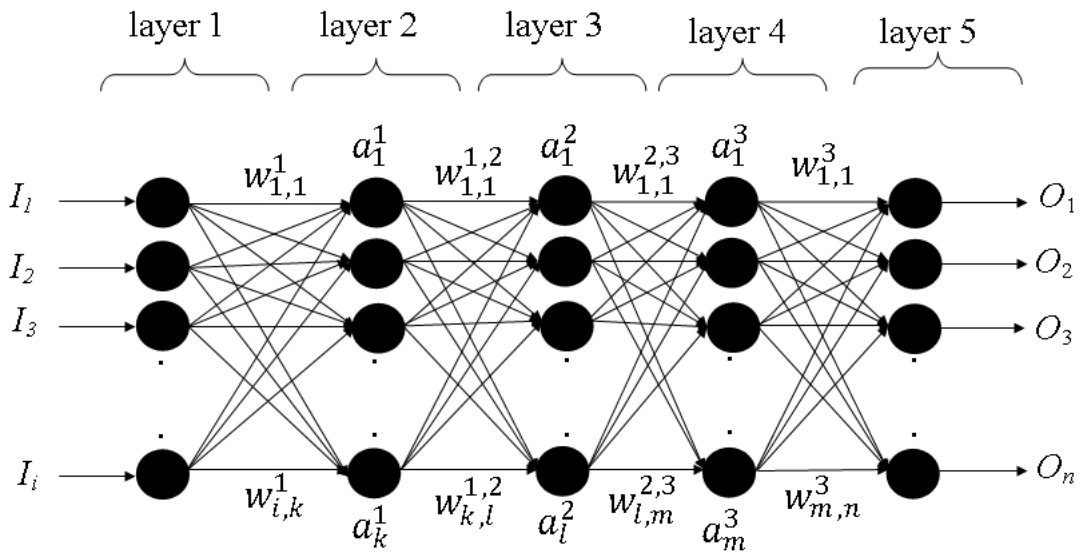

Figure 2.13.: Multi layer

- Multiple Layer

Multiple layers neuron is slightly different from single layer neurons. It can have one or more hidden layers between the output and input signals. This architecture has been applied successfully to solve some difficult and diverse problem such as in modelling, prediction and pattern classification [33]. Basically, the architecture of FFNN consists of three layers, one input layer, one hidden layer and one output layer.

Figure 2.13 consists of five layers; one input layer at layer 1, three hidden layers at layer 2 to 4 and one output layer at layer 5. The input layer receives the inputs signal I_i and goes through to the hidden layers at layer 2 along with weight $W^1_{i,k}$ to obtain the signal a^1_k. These signal move forward with weight $W^{1,2}_{k,l}$ to obtain a^2_l at layer 3. Same process is employed to obtain signal a^3_m at layer 4. The signal a^3_m with weight $W^3_{m,n}$ move forward to give output signal O. Typically, this type is popular but is quite complex because of numerous neurons connection.

2.5.3. Multiple Layer Perceptron

A Multiple layer perceptron network or some called multiple layer feed-forward neural network (FFNN) or Multiple Layer Neuron which is one of the most popular and successful neural network architectures. It is suitable for a wide range of applications such as prediction, process modelling, recognition and so on. [37, 38, 39]. Basically, the MLP consists of three layers;

1. an input layer which receives the input signal,

2. a hidden layer which processes the data and sends the signal to the output layer,

3. an output layer which generates the output signal as a result.

In other words, each unit will receive the input signals (I_i) directly and send to hidden layers. Then, hidden signals (a_j) are moved forward to the output layers to generate the output signals (O_i). In every layer contains neurons where each neuron is connected to other neurons via weight connections as illustrated in Fig. 2.14. Mathematically, the typical FFNN can be interpreted by using the following equations.

$$\nu_j = \sum_{i=1}^{m} I_i w_{ij} + \theta_j \tag{2.18}$$

$$a_j = \theta\left(\nu_j\right) = \frac{1}{1 + exp\left(-\nu_j\right)} \tag{2.19}$$

$$O_k = \theta\left(\nu_k\right) = \sum_{j=1}^{n} a_j w_{jk} + \theta_k \tag{2.20}$$

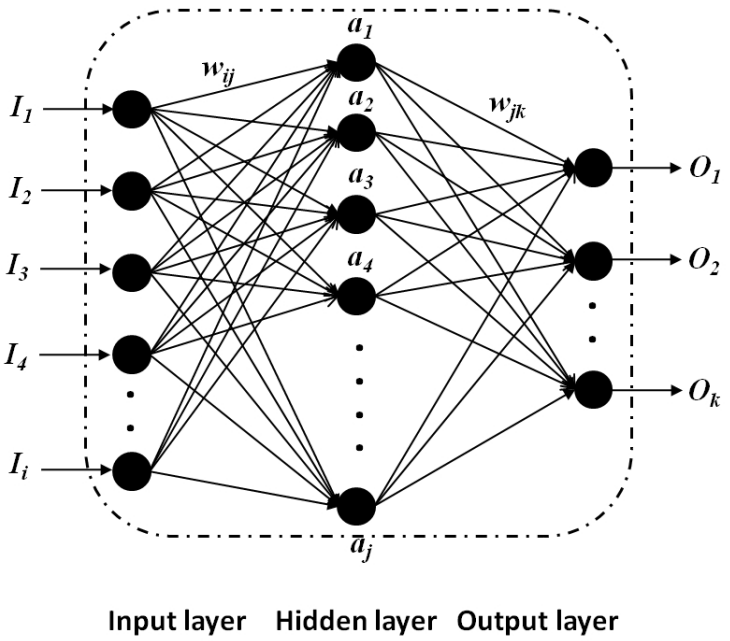

Figure 2.14.: Architecture of FFNN

$$E = \frac{1}{N} \sum_{k=1}^{N} (D_k - O_k)^2 \tag{2.21}$$

Therein, E is an error term, D_r stands for a desired value (target), and O_k represents the output signal (network output), N signifies the number of samples, ν_j is the summation of I_i (input signal), w_{ij} denotes a weight value between the input and hidden layer, and ϑ_j represents the bias/threshold at j-th. Furthermore,a_j signifies the output of the hidden layer, $\varphi(\nu_j)$ denotes the transfer function (sigmoid function) associated with node j in the hidden layer, O_k represents the output of the output layer, $\varphi(\nu_k)$ stands for the transfer function of the output layer, but in this case, we used a linear function ($\varphi(\nu_k) = \nu_k$). Other variables are w_{jk}, which is the weight value between hidden and output layers, ϑ_k is the bias at output layer at k-th. i , j and k respectively denote the input nodes ($i = 1, \ldots, m$) in the input layer, ($j = 1, \ldots, n$) are the hidden nodes in the hidden layer, and ($k = 1, \ldots, q$) is the output node in the output layer.

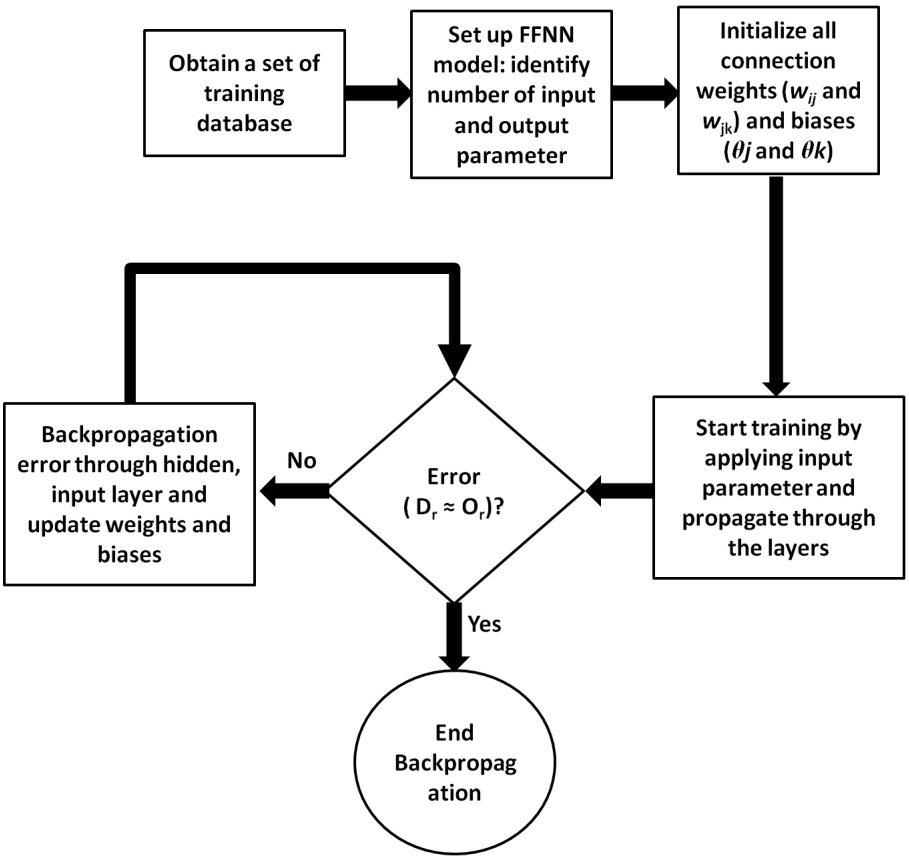

Figure 2.15.: Flow of backpropagation

2.5.4. Backpropagation

Backpropagation developed by Rumelhart et al. [40] was created by generalizing the Widow-Hoff learning rule to multiple layers network and nonlinear differentiable transfer function [41]. The backpropagation learning algorithm was one of the earliest and the most common method for training FFNN. It was used to train multiple layers network to solve difficult and diverse problems. This algorithm is a learning scheme where the error is back propagated layer by layer and used to update the weight.

Figure 2.15 illustrates the backpropagation algorithm process. The implementation of this algorithm involves two steps;

1. Database is required for backpropagation training purpose. Then, identify the number of input and output neuron to set up the FFNN architecture.

Using the initialized weight and bias, the input parameters are transmitted from the input layer through the hidden layers to the output layer. The values (O_k) obtained from the output layer are compared with the desired output (D_r). Therefore, the prediction errors will be available.

2. This stage involves propagating these prediction errors backward from output layer through the hidden layers to the input layer. The amount of weights and biases are compared during this process and the initialized bias and weight are updated. These processes are repeated until the weight and biases converge and the prediction output approximates the desired output.

2.5.4.1. Levenberg-Marquardt Learning Algorithms

Levernberg-Marquardt algorithm was proposed by Levenberg [42] and Marquardt [43]. This algorithm is combined the excellent local convergent properties of the Gauss-Newton near a minimum with the consistent error decrease provided by gradient descent far from a solution [33]. It was designed to approach a second order training speed without computing the Hessian matrix. The Levenberg-Marquardt can be approximated as

$$w_{i+1} = w_i - \left[J^T(w)\,J(w) + \eta I\right]^{-1} J^T(w)\,e(w) \tag{2.22}$$

where $e(w)$ is a function containing the individual error terms, $J(w)$ presents the Jacobian matrix, I denotes the identify unit matrix, and η stands a scalar that controls the size of the trust region. When $\eta = 0$ the method become equivalent to the Gauss-Newton method whereas for every large η the Levenberg-Marquardt tends to gradient descent with very small step size [35]. In this way, the performance of the sum of square (Ref: Eq. 2.21) can be reduced.

In FFNN, there are many kinds of training algorithms such as gradient descent, gradient descent with momentum, resilient back-propagation with flectcher-reever update and so on. However, a study by R. Sing et al. [44] and A. Saengrung et al. [45] found that the Levenberg-Marquardt is faster process than other algorithms with good accuracy predictions.

2.6. Dimension Vision Predictor (DVP)

2.6.1. Stereo Vision Analogy

There are several techniques used to measure dimensions with a camera [46, 47]. Unfortunately, some techniques demand special equipment and camera lens calibration. Therefore, aiming for practical use, this study chooses survey-from-photo [48] because it can be implemented directly from any ordinary camera without calibrating the camera lens.

Generally, survey-from-photo identifies the dimension based on two images. The images are marked with two corresponding points. Then both are connected to make a line at an object to measure. To achieve an accurate measurement, a reference dimension is necessary. The reference dimension is a dimension obtained from an object that is known exactly. Here, survey-from-photo uses that object dimension as a reference to standardize the scale range to the images.

The basic concept of survey-from-photo is is derived from the "stereo vision" principle, which uses two cameras to measure dimensions of an object, as presented in Fig. 2.16. One camera is located at C_r and another at C_l with intervening distance (d). The cameras are focused at point $P_1(x_1, y_1, z_1)$ and $P_2(x_2, y_2, z_2)$ with certain focus length (f), which is are all obtainable at the

camera lens. At f, two image points are apparent at the image P_{1r}, P_{1l}, P_{2r}, P_{2l} with respective coordinates (x_{1r}, y_{1r}), (x_{1l}, y_{1l}), (x_{2r}, y_{2r}), and (x_{2l}, y_{2l}). The coordinate (x_{1r}, y_{1r}), (x_{1l}, y_{1l}), (x_{2r}, y_{2r}), and (x_{2l}, y_{2l}) are calculable by considering the center of image as the origin. To obtain the coordinate of $P_1(x_1, y_1, z_1)$ and $P_2(x_2, y_2, z_2)$, the equation is definable simply as shown below.

$$P_1\left(x_1, y_1, z_1\right)\begin{pmatrix} x_1 \\ y_1 \\ z_1 \end{pmatrix} = \frac{d}{x_{1l} - x_{1r}}\begin{pmatrix} x_{1l} \\ y_{1l} \\ f \end{pmatrix} \tag{2.23}$$

$$P_2\left(x_2, y_2, z_2\right)\begin{pmatrix} x_2 \\ y_2 \\ z_2 \end{pmatrix} = \frac{d}{x_{2l} - x_{2r}}\begin{pmatrix} x_{2l} \\ y_{2l} \\ f \end{pmatrix} \tag{2.24}$$

$$L_x = d\left(\frac{x_{1l}}{x_{1l} - x_{1r}} - \frac{x_{2l}}{x_{2l} - x_{2r}}\right) \tag{2.25}$$

$$L_y = d\left(\frac{y_{1l}}{x_{1l} - x_{1r}} - \frac{y_{2l}}{x_{2l} - x_{2r}}\right) \tag{2.26}$$

$$L_z = df\left(\frac{1}{x_{2l} - x_{2r}} - \frac{1}{x_{2l} - x_{2r}}\right) \tag{2.27}$$

In those equations,

$$x_{1l} = \frac{f}{\tan\theta_{P_{1l}}} \tag{2.28}$$

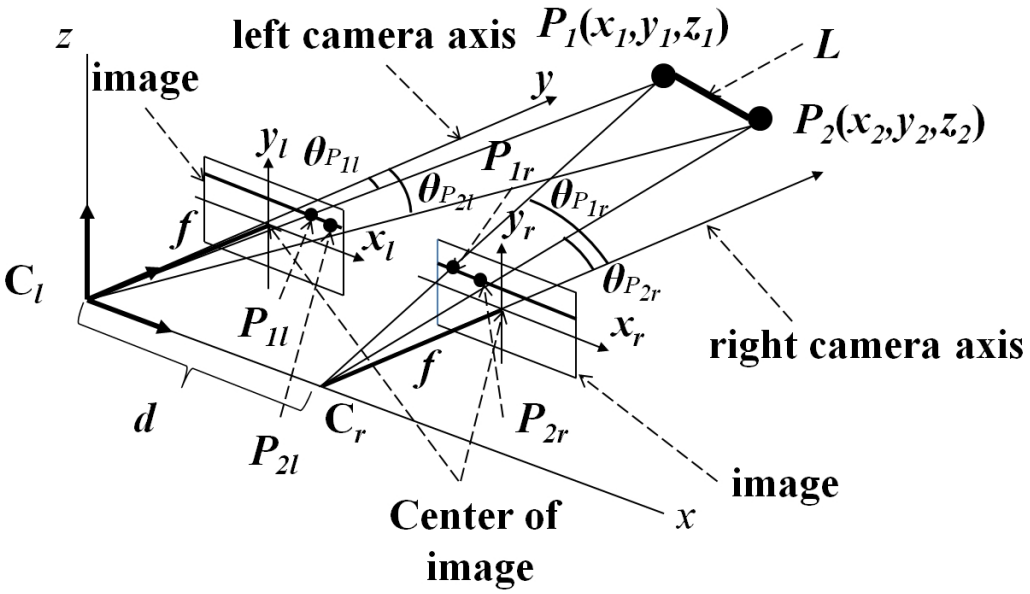

Figure 2.16.: Principle of stereo vision

$$x_{2l} = \frac{f}{\tan\theta_{P_{2l}}} \tag{2.29}$$

$$x_{1r} = \frac{f}{\tan\theta_{P_{1r}}} \tag{2.30}$$

$$x_{2r} = \frac{f}{\tan\theta_{P_{2r}}} \tag{2.31}$$

The distance (L) between P_1 and P_2 can be expressed as;

$$L = \sqrt{(L_x)^2 + (L_y)^2 + (L_z)^2} \tag{2.32}$$

Using the reference scale (L), DVP is identifiable by coordinates at P_{1r}, P_{1l}, P_{2r}, and P_{2l} by clicking the mouse.

2.7. Finite Element Analysis (FEA)

The FEA numerical technique, well known in acoustical fields, has been used in many fields to obtain the sound field of rooms with high accuracy [49, 50]. The benefits of using FEM are: to provide a simulation form, have the ability to analyze non-homogeneous material and can preserve a very dynamic, linear or nonlinear data [51]. The important thing is FEM is reliable in low frequency (125 kHz to 1 kHz) rather than ray tracing (2 kHz to 16 kHz) but it will be confirmed in the next stage. For this study, the FEA technique is time domain analysis.

The FEA procedure is based on the principle of the minimum of total potential energy applied to a three-dimensional sound field. The discretized equation for a sound field in the frequency domain is expressed as

$$\left(\mathbf{K} + i\omega\mathbf{C} - \omega^2\mathbf{M}\right)\mathbf{p} = i\omega\rho\nu_0\mathbf{W} \tag{2.33}$$

where $\mathbf{M}$, $\mathbf{C}$, and $\mathbf{K}$ respectively signify the acoustic mass, dissipation, and stiffness matrices. Furthermore, i, $\mathbf{p}$, ρ, ω, v_0, and $\mathbf{W}$ respectively denote the imaginary unit ($i^2 = -1$) sound pressure vector, the air density, angular frequency, velocity of sound vibration and distribution vector. By assuming that $\dot{}$ and $\ddot{}$ are first-order and second-order derivatives in time, the semi discrete equation in time domain can be evaluated using Eq. 2.34 shown below.

$$\mathbf{M}\ddot{\mathbf{p}}+\mathbf{C}\dot{\mathbf{p}} + \mathbf{K}\mathbf{p} = \rho\dot{\nu_0}\mathbf{W} \tag{2.34}$$

To calculate the equation 2.34, the Newmark β [52] scheme is used to solve step by step as shown below;

$$\mathbf{p}' = \mathbf{p}'_n + \triangle t\dot{\mathbf{p}}'_n + \frac{\triangle t^2}{2}\left[(1-2\beta_H)\,\ddot{\mathbf{p}}'_n + 2\beta_H\ddot{\mathbf{p}}'_{n+1}\right] \tag{2.35}$$

$$\dot{\mathbf{p}}'_{n+1} = \dot{\mathbf{p}}'_n + \triangle t\left[(1-\gamma_H)\,\ddot{\mathbf{p}}'_n + \gamma_H\ddot{\mathbf{p}}'_{n+1}\right] \tag{2.36}$$

where n and Δt is respectively denotes the time step counter, the time step value. β_H and γ_H are integration parameters. While $\mathbf{p}'$ is the vector of unknowns at the finite element node, $\dot{\mathbf{p}}'$ and $\ddot{\mathbf{p}}'$ are first and second derivative with respect to time. Further explanation, time domain analysis on this study is described elsewhere by following this paper [8].

2.8. Summary

The techniques discussed above are used for identifying the material surfaces and room dimensions. Such techniques are also used for simulating sound fields of rooms, and the uses of these techniques will be discussed in the next chapter.

Chapter 3.

Development of System 1 to Identify Material Surfaces

3.1. Introduction

This chapter discusses the development of System 1. To identify the material surface, six types of material surfaces are captured by using an ordinary camera. Using GLCM, all the images are computed in order to obtain Haralick's Coefficients. Then, those coefficients are used as input parameters for FFNN to identify the material surfaces and at the same time absorption coefficients are provided.

There are three stages to develop this system;

1. Material Surfaces capturing,
2. GLCM and Haralick's Coefficient Implementation, and
3. FFNN Implementation.

Table 3.1.: Propotion of the surface images

Surface	Type of surface image	No. of image
(a)	wall	69
(b)	door	71
(c)	floor	66
(d)	window	56
(e)	ceiling	67
(f)	carpet	40

These stages are discussed in subsections below. The reliability of material surfaces estimations are presented at results subsection.

3.2. Methodology of System 1

3.2.1. Material Surface Capturing

For this study, six material surfaces were taken of Oita University rooms, as portrayed in Fig. 3.1. Surfaces (a), (b), (c), (d), (e), and (f) are, respectively, surfaces for walls, doors, floors, windows, ceilings, and carpets.

In order to perform material surfaces capturing, an ordinary camera is useful. Regarding standardization of images, a digital single-lens reflex (DSLR) camera with Sigma 50 mm f2.8 lens was used as illustrated in Fig. 3.2. In addition, the distance from the camera to the surface material was set to 40 mm with autofocus mode, whereas the respective lens settings for aperture, shutter speed and ISO speed were f2.8, 1/80, and 100. To analyze the accuracy of System 1, 368 images of surfaces were captured at different locations in three rooms. The proportions of images of material surfaces are shown in Table 3.1. Then, all images were analyzed using GLCM.

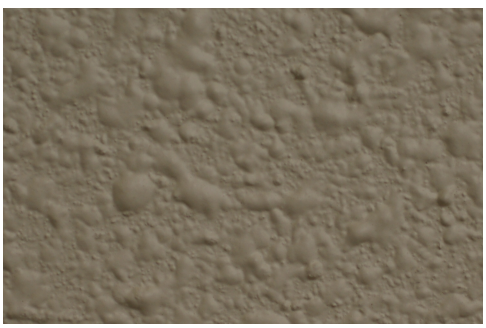

(a) wall

(b) door

(c) floor

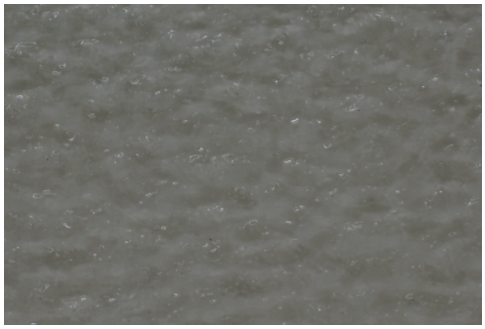

(d) window

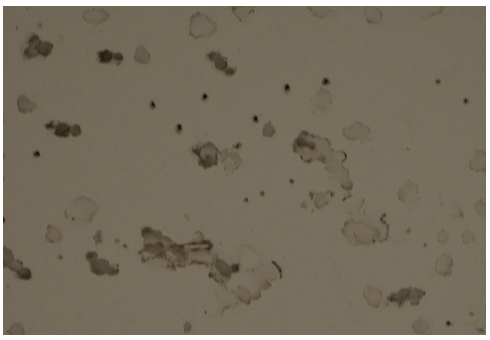

(e) ceiling

(f) carpet

Figure 3.1.: Sample of surface images

Figure 3.2.: Sigma 50 mm:f 2.8 lens

3.2.2. Gray Level Co-Occurrence Matrix and Haralick Coefficients Implementation

The GLCM was computed for the 368 images of material surfaces using the following settings: i. d =1, $\theta = 0°$; ii. d = 1, $\theta = 45°$; iii. $d = 1$, $\theta = 90°$; and iv. $d = 1$, $\theta = 135°$. The GLCM computations started when all the surface images were transformed into gray scale image as presented in Fig. 3.3.

Regarding to the following setting as mentioned above, each surface images were provided four types of GLCM. In subchapter 2.4 explained that GLCM is hard to use directly, therefore we used Haralick's coefficient to transform the GLCM into statistcal approach [26]. Each Haralick's coefficient provides four values based on setting, but only an average value of four values were considered hereinafter. Table 3.2 (a) shows example of four values for each Haralick coeffient at each surface image and Table 3.2 (b) is the average value from four values.

The average value is designated as the coefficient value for this study.

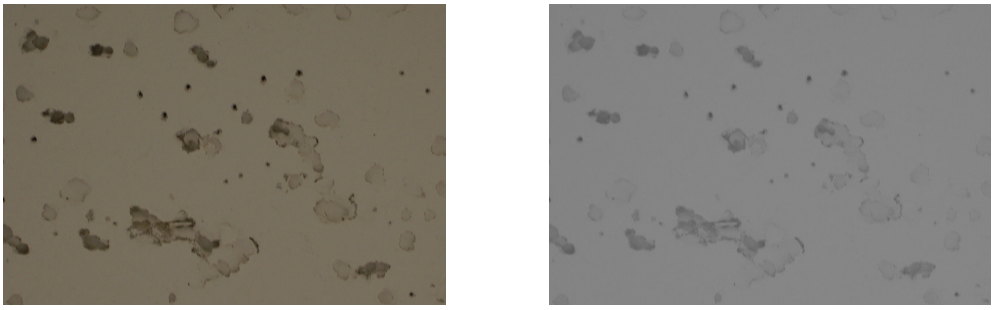

(a) (b)

Figure 3.3.: Transformation from colour image to gray image (a) colour surface image (b) gray surface image

(a)

θ	*cont*	*corr*	*ASM*	*hom*
0°	0.1680	0.6495	0.3809	0.9160
45°	0.2413	0.4975	0.3370	0.8794
90°	0.2421	0.4949	0.3374	0.8789
135°	0.2598	0.4590	0.3278	0.8701

(b)

cont	*corr*	*ASM*	*hom*
0.2278	0.5252	0.4557	0.8861

Table 3.2.: Example of Haralick coefficient value of a surface image (a) Four values depending onto θ for each Haralick' coefficient (b) average value from four values

Because of variations of brightness and texture features in our experiment, the ranges of the coefficient values become too wide to be processed. To overcome this problem, a limitation for each coefficient value was made using the means ($\bar{x}$) and standard deviation (σ). The limitations are ($\bar{x} - \sigma$) and ($\bar{x} + \sigma$), respectively, for low limitation and high limitation. The coefficient values beyond the limitations were removed from further investigation.

3.2.2.1. Programming of Gray Level Co-Occurrence Matrix and Haralick Coefficients

To obtain the entire of Haralick coefficient for each image surface, the author used MATLAB Release 2010 [53] with image processing toolbox [54] to developed a programming. The programming can be referred at Appendix I. This programming consists of four paragraphs;

- Paragraph 1

This paragraph is used to load the images of material surfaces. If the images are 10, thus we have to load all the images into the MATLAB workspace.

- Paragraph 2

Third paragraph is used to convert the image into greyscale.

- Paragraph 3

Four paragraph is used to develop the GLCM for the images. The coding "*offset* = [0 1;-1 1;-1 0;-1 -1];" are proposed by MATLAB which indicated the direction d and θ; d =1, $\theta = 0°$; ii. d = 1, $\theta = 45°$; iii. $d = 1$, $\theta = 90°$ and iv. d = 1, $\theta = 135°$. The Figure 3.4 illustrates the relationships of directions that are defined by the offsets, where 1 is the distance from pixel of origin. Then, using

graycomatrix the matrix of GLCM for each image is developed.

- Paragraph 5

Finally, from GLCM the Haraliks' coefficients are obtained by using *graycoprops* which provided four coefficients; *Contrast, Correlation, Energy* or *ASM,* and *Homogeneity*

3.2.3. Results of Gray Level Cooccurrence Matrix

As mentioned in subsection 3.2.2, all the surface images (368) were fed into GLCM and analysis using Haralick coefficient. In Fig. 3.5 illustrated the range of four coefficient values for six surface. It shows that the range for each coefficient in each surface image is too wide to process some of them almost similar (e.g. wall $\approx$ window $\approx$ ceiling; door $\approx$ floor). Thus, the author used limitation to distingush the range to make easy FFNN recognizes the surface images during the during process.

Figure 3.6 portrays the range of four coefficient values for the six surface images after limitation. Each coefficient value showed a limitation. The limitation shows two bars at the top and below represented as a high limitation (HL) and low limitation (LL). Intermediate of the high and low limitation is a medium limitation (ML). Observation reveals that all surface images gave different coefficient values, except surfaces (b) and (c). Both showed approximately similar coefficient values for all coefficients. To overcome the redundancy of coefficient values during FFNN learning, both were combined to the same surface image.

Results of analyses indicate that only 53.8% of 360 images of surfaces (surface wall = 39 surface images, surface door = 50 surface images, surface floor = 27 surface images, surface window = 26 surface images, surface ceiling = 30

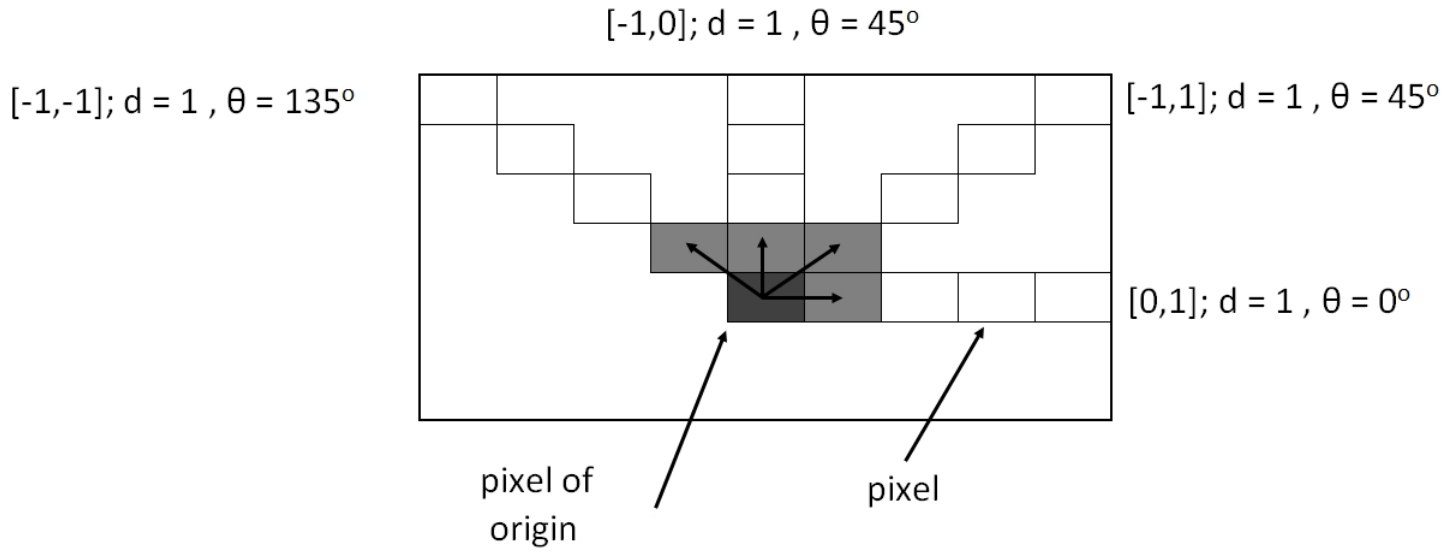

Figure 3.4.: Relationships between offset and direction d and θ

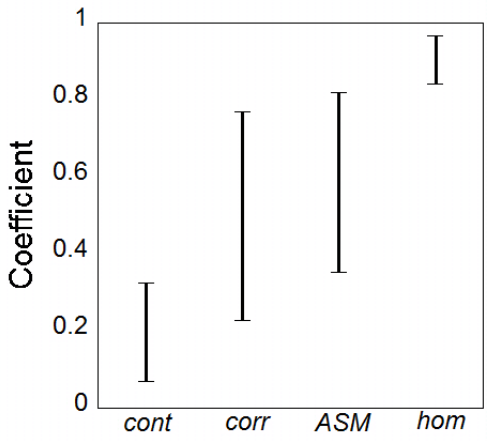

(a) wall

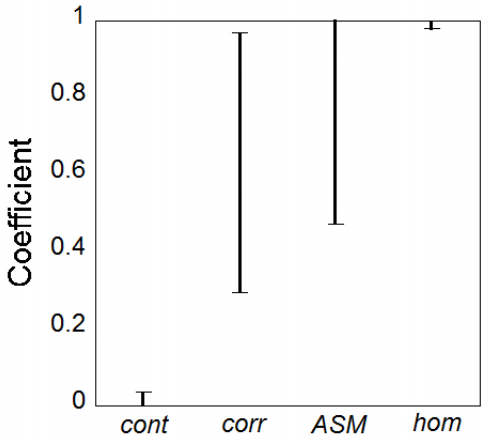

(b) door

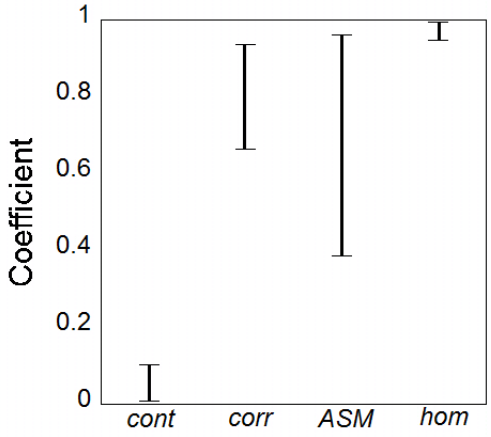

(c) floor

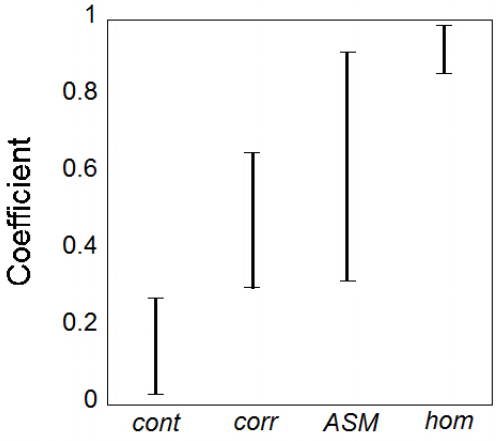

(d) window

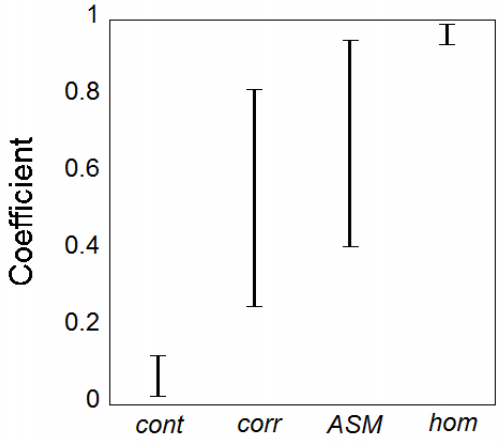

(e) ceiling

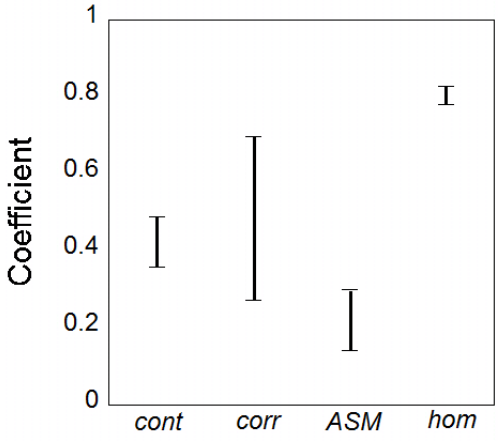

(f) carpet

Figure 3.5.: Range of coefficient values for six surface images

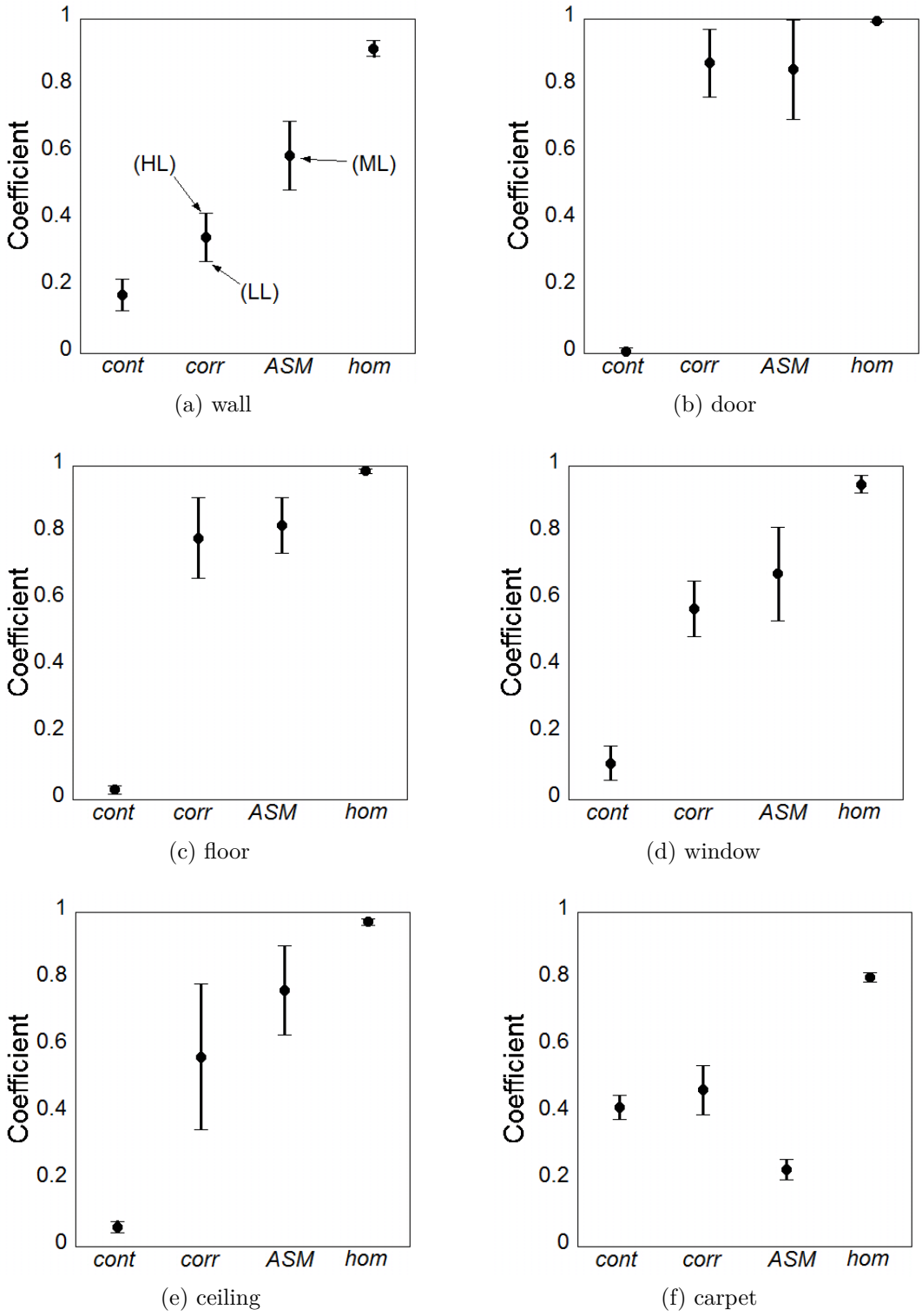

(a) wall (b) door

(c) floor (d) window

(e) ceiling (f) carpet

Figure 3.6.: Limitation of coefficient values for six surface images

surface images, and surface carpet = 20 surface images) were used for FFNN because of limitations.

3.2.4. Feed Forward Neural Network Implementation

3.2.4.1. Identification of training database

To develop FFNN, input and output parameters are four coefficients values (*cont*, *corr*, *ASM*, and *hom*) and material surfaces respectively. In this study, the absorption coefficients (α) of six material surfaces are referred from reports of the relevant literature [55, 56] as shown in Table 3.3. Therefore, by identifying the material surfaces, we are able to ascertain the absorption coefficients of surfaces simultaneously. To identify the material surfaces, we used a classification number (1–5) to represent the output parameter. Table 3.4 - 3.9 show the range descriptions of input parameters and output parameters for each material surfaces. As mention earlier, material surface of door (Ref: Table 3.5) and floor (Ref: Table 3.6) were combined because both indicated approximately similar in all coefficient values. Thus, the outputs for both were 2. The combination was necessary because FFNN unable estimated correctly if the coefficient values for two surface materials were similar. The total surface images used are 194 after limitation for developing the FFNN.

Table 3.3.: Absorption coefficient for each material surface

Type of surfaces	absorption coefficient
wall	0.07
door	0.02
floor	0.02
window	0.04
ceiling	0.4
carpet	0.06

Table 3.4.: Range description of coefficient values for wall

type of surfaces	input parameter			output parameter
	coefficient	min	max	classification no.
wall	cont	0.1292	0.2234	1
	corr	0.2747	0.4194	
	ASM	0.4897	0.6948	
	hom	0.8888	0.9354	

Table 3.5.: Range description of coefficient values for door

type of surfaces	input parameter			output parameter
	coefficient	min	max	classification no.
door	cont	0.0003	0.01795	2
	corr	0.7674	0.9691	
	ASM	0.6994	0.9983	
	hom	0.9910	0.9998	

Table 3.6.: Range description of coefficient values for floor

type of surfaces	input parameter			output parameter
	coefficient	min	max	classification no.
floor	cont	0.0163	0.0425	2
	corr	0.6627	0.9058	
	ASM	0.7398	0.9048	
	hom	0.9788	0.9918	

Table 3.7.: Range description of coefficient values for window

type of surfaces	input parameter			output parameter
	coefficient	min	max	classification no.
window	cont	0.0578	0.1613	3
	corr	0.4889	0.6546	
	ASM	0.5376	0.8166	
	hom	0.9194	0.9611	

Table 3.8.: Range description of coefficient values for ceiling

type of surfaces	input parameter			output parameter
	coefficient	min	max	classification no.
ceiling	cont	0.0411	0.0763	4
	corr	0.3502	0.7865	
	ASM	0.6328	0.8997	
	hom	0.9623	0.9799	

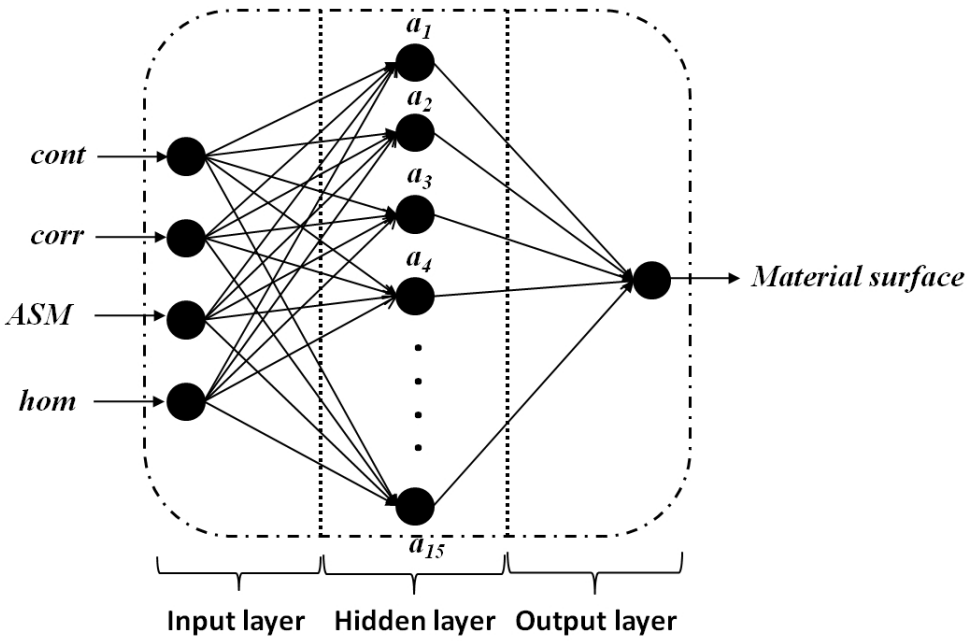

Figure 3.7.: Architecture of FFNN for System 1

Table 3.9.: Range description of coefficient values for carpet

type of surfaces	input parameter			output parameter
	coefficient	min	max	classification no.
carpet	cont	0.3810	0.4524	5
	corr	0.3942	0.5427	
	ASM	0.1996	0.2625	
	hom	0.7925	0.8188	

3.2.4.2. Training Phase

Coefficient values in the limitation were fed into FFNN. Four coefficients (*cont*, *corr*, *ASM*, and *hom*) and the material surfaces were used respectively as input neurons and output neurons. The numbers of hidden neuron were set up from 2 to 15 . The architecture of FFNN in this stage is shown in Fig. 3.7.

Before implementing the FFNN, database contains of coefficient values and types of material surface are transformed from 0.1 to 0.9 using Eq. 3.1 to standardize the range.

$$x_t = 0.1 + \left[0.8 \times \left(\frac{x_o - x_{min}}{x_{max} - x_{min}}\right)\right] \tag{3.1}$$

where, x_o is the original database, x_t is the transform database, x_{min} and x_{max} is the minimum and maximum of the original database, respectively.

The database was seperated into three subsets a training subset, a validation subset, and a testing subset. The proportion of each subset is 60% of database for training subset, 20% of database for validate subset and 20% of database for testing subset.

In addition, the learning algorithm in this study was Levenberg–Marquardt (trainlm) because it is faster and more efficient [36, 57, 45, 44]. To obtain the optimum network, trial and error scheme was conducted by combining all those neurons (e.g. [i; h; o] for [number of input nueron; number of hidden neuron; number of output neuron]; example combination [4; 6; 1], [4; 10; 1], ... or [4; 9; 1]) with the number of hidden neuron used were from 2 to 15, but only one combination that provided good performance was selected.

The optimum network can be obtained when learning process in done. Neverthless during the process, 'over training' or 'under training' may occur and this will affect to the idenfication accuracy. The best way to avoid this problem is to use 'earling stopping' [58, 59, 33]. Three subsets of database as mention above were used to apply the early stopping process . The function of those subsets; training subset is used to train the FFNN, validation subset is used to validate the learning process, and the testing subset is used to investigate the prediction performance. There are no specific proportions of subsets were set. At this point, the proportions of subsets were chosen arbitrarily as apply above. Generally, the training subset should be larger than the validation susbset and testing subset (e.g. 60% training, 20% validation, 20% testing [41]; 50% training,

25% validation, 25% testing [60]; 60% training, 15% validation, 25% testing [61]; 72% training, 13% validation, 15% testing [62]). For the assessment, the mean square error (MSE) and correlation coefficients (R) are used. The network that gives minimum MSE and high correlation R is selected as the optimum network. The equations of MSE and R are stated as follows;

$$MSE = \sum_{i=1}^{N} (e_i)^2 = \sum_{i=1}^{N} (t_i - a_i)^2 \tag{3.2}$$

where e_i is error, t_i is desired value, a_i is actual value and N is number of data.

$$R = \frac{\sum_{i=1}^{N} (x_i - \bar{x})(y_i - \bar{y})}{\sqrt{\sum_{i=1}^{N} (x_i - \bar{x})^2} \sqrt{\sum_{i=1}^{N} (y_i - \bar{y})^2}} \tag{3.3}$$

where x_i is the actual values, y_i is predicted values, $\bar{x}$ and $\bar{y}$ are the mean values.

3.2.4.3. Programming of FFNN

To develop the FFNN, in this study used MATLAB Release 2010 [53] with Neural Network toolbox [41] as a tool to create the FFNN programming. The programming for FFNN can be referred at Appendix II. This programming consists of four paragraph of steps;

- Paragraph 1

In this paragraph, database is loaded into the workspace using load *trainnorm2.txt* (able uses any kind of file name). The database is seperated by input parameters which are *P1*, *P2*, *P3* and *P4* for coefficient values of *contrast*, *correlation*, *ASM* and *homogeinity*, respectively. While output paramter *T1* is type of material surface.

- Paragraph 2

In this level, database is normalized by scaling it to between 0.1 and 0.9 for data simplification. Then, we organize the input parameters (*P1*, *P2*, *P3* and *P4*) into P and output parameter (*T1*) to T. Afterthat, the database is separated into 3 subsets, that are training subset (60% of database (e.g. 168 database)), validation subset (20% of database) and testing subset (20% of database). These subsets are defined as *trP1*, $v.P$ and $t.P$, respectively, for input training subset, input validation subset and input testing subset. The *trT1*, $v.T$ and $t.T$ are defined as output training subset, output validation subset and output testing subset.

- Paragraph 3

In this stage, number of hidden neuron is denoted by *s1*. Value of *s1* depends on the user input. As mentioned, in this study used 2 - 15 hidden neurons The first step is to create a FFNN architecture. The coding is shown below:

net=newff(minmax(trP1),[S1 1],{'tansig','purelin'},'trainlm')

The word *newff* means the network is created using feed-forward type and 1 indicates that the network considers only one output. Function minmax is used to determine the range of the inputs. The *'tansig'*,'pureline' and *trainlm* are the type of transfer function and training algorithm. The network will initialise the weight and bias before being trained. The network is initialised by:

net=init(net);

tic,[net,tr]=train(net,trP1,trT1,[],[],v,t);toc;

Therefore, the network is ready to be trained. During the training, the weight and bias of the network are iteratively adjusted to find optimum network.

The early stopping method used in this stage functions to avoid over learning or under learning which will affect the network performance.

- Paragraph 4

In this stage, the neural network has been created and ready to be used for predictions. The prediction value is simulated after finishing the training phase. The predicted values are compared with the output data for error identification. The MSE in training (*per_train*), validation (*per_validate*) and testing (*per_testing*) subset can be determined based on the error from each subset. The R can be plotted to show the prediction value compared with the actual value.

3.2.5. Results of Feed Forward Neural Network

As mention before, to obtain the optimum network, trial and error was applied in this study. We used 2 to 15 number hidden neurons. Each number of hidden neuron was trained to obtain the MSE. Subsequently, MSE for each hidden neuron was compared to identify the minimum MSE. The number of hidden neuron indicates a minimum MSE was selected as optimum network. In this case, we choose the minimum MSE at validation subset because validation error brings information the performance of FFNN.

Table 3.10 shows the MSE of each subset in each hidden neuron. In the validation subset, it seems that the number of hidden neuron of 6 gives minimum MSE of 0.0017 compared than others. Although, MSE at training subset gives 0.0018, which is not a minimum MSE, but it can be accepted because the range between 0.0018 and minimum MSE of 0.0017 is approximate closer.

From the analysis, the optimum network [4,6,1] represents number of input neuron, hidden neurons and output neuron respectively with MSE ≤ 0.0018 and correlation coefficient R ≥ 0.9 (Figure 3.8 and 3.9) was obtained for both

Table 3.10.: MSE of each number of hidden neuron

number of hidden neuron	MSE	
	training subset	validation subsets
2	0.0180	0.0101
3	0.0059	0.0060
4	0.0034	0.0046
5	0.0030	0.0040
6	0.0018	0.0017
7	0.0017	0.0032
8	0.0034	0.0021
9	0.0017	0.0019
10	0.0032	0.0020
11	0.0017	0.0022
12	0.0018	0.0022
13	0.0020	0.0018
14	0.0030	0.0023
15	0.0018	0.0034

training and validation subsets.

To confirm their performance, we used 39 surface image of the testing subset. By using this optimum network, it shows the MSE = 0.0075 with the correlation coefficient R $\geq$ 0.9 as shown in Figure 3.10. The result from testing subset, it can be assumed that System 1 performance is inferred to be good at this stage.

3.3. Summary

At this stage, the System 1 was well developed. The optimum network is obtained from the number of hidden neuron of 6. The MSE for training subset and validation subset for both is MSE $\leq$ 0.0018 and correlation coefficient R $\geq$ 0.9. By using the testing subset, the optimum network obtained good estimation performance with MSE = 0.0075 with the correlation coefficient R $\geq$ 0.9. As mention earlier, the output of the network was the classification number from 1 to 5. Each number represents the type of material surfaces. By these numbers, we

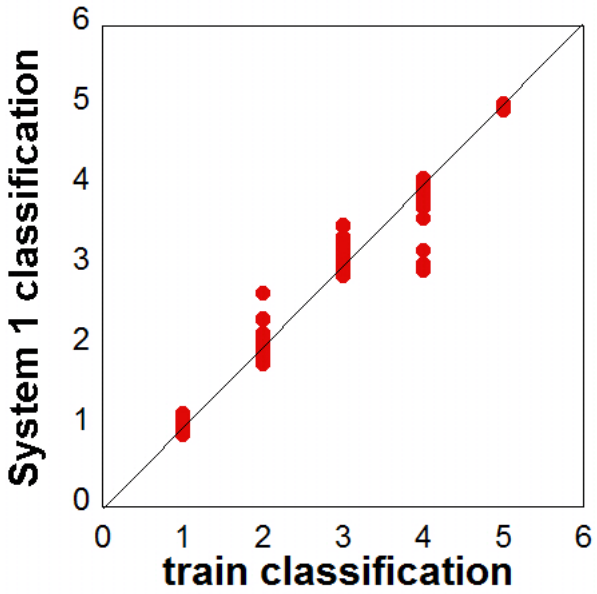

Figure 3.8.: Comparison System 1 classification between train classification

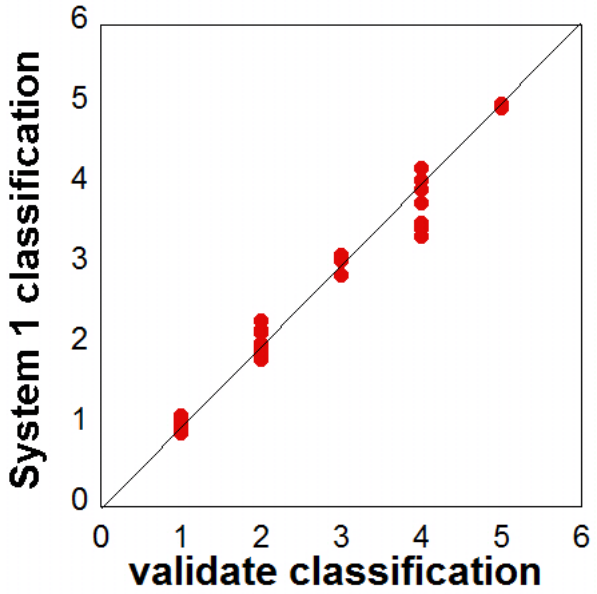

Figure 3.9.: Comparison System 1 classification between validate classification

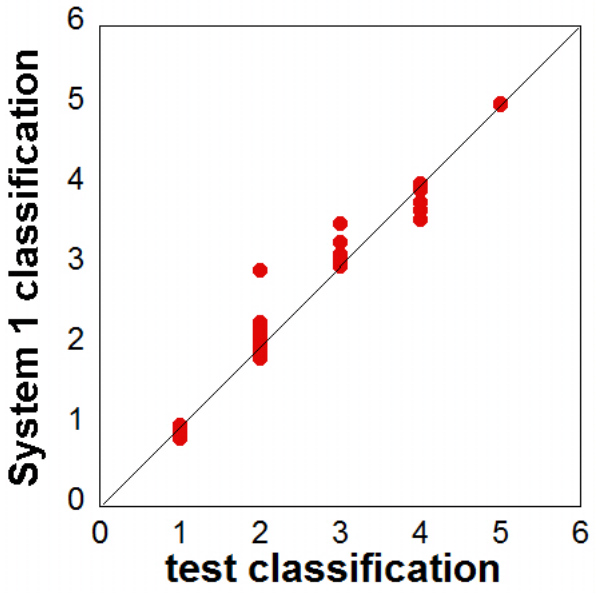

Figure 3.10.: Comparison System 1 classification between test classification

able indicate the material surfaces, and the absorption coefficients are recognized simultaneously by referring the Table 3.3.

Chapter 4.

Development of System 2 to Identify Dimensions

4.1. Introduction

This chapter discusses the development of System 2. To identify dimensions, two images at one view with contains of objects that want to measure are captured using the same camera at System 1. Then, DVP computes the objects in the images in order to measure the dimensions. In this work, there are two stages to develop this system;

1. Image Capturing, and

2. DVP Implemenation

These stages are discussed in subsections below. To investigate the repeatability, 100 dimensions at several objects are used. This part is explained at results subsection.

(a)

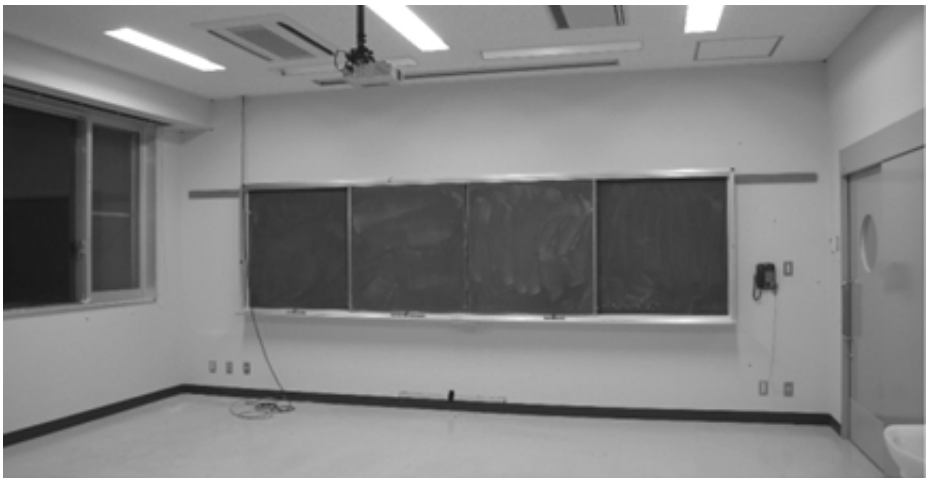

(b)

Figure 4.1.: Example of two images at one view (a) left image (b) right image

4.2. Methodology of System 2

4.2.1. Image Capturing

The same camera for System 1 was used with focus lenses of 18–70 mm to capture two images at one view. The camera was set in auto focus mode. Figure 4.1 shows an example of two images that captured by the camera at one view. Two images are left image and right image which is indicated the position of the camera captured. That view at the images supposedly displays the objects to be measured. Then, the images are feed into DVP to measure the target objects.

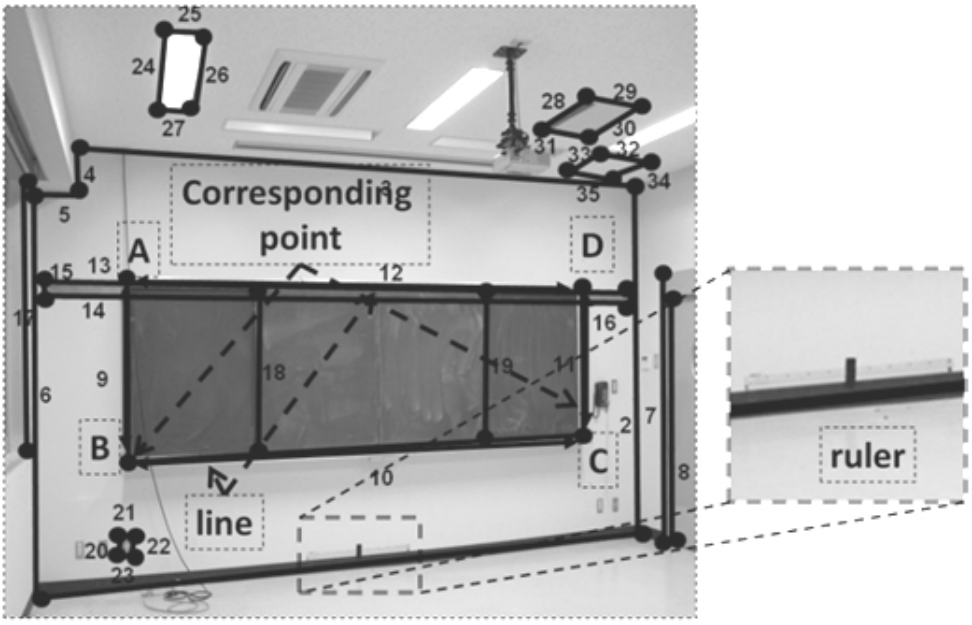

(a)

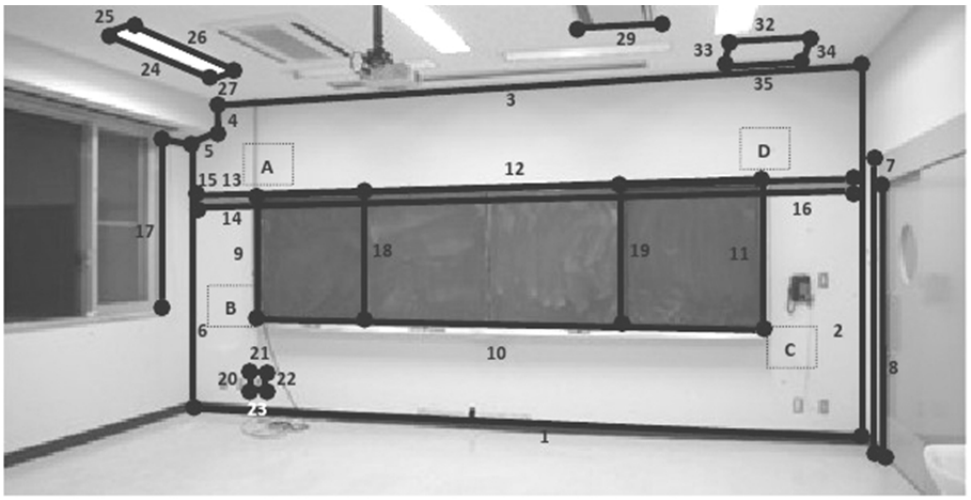

(b)

Figure 4.2.: Identification dimension using ruler methods in two image; (a) Left image (b) Right image

4.2.2. Dimension Vision Predictor Implementation

Figure 6 presents an example of identifying dimensions of objects in two images at one view. Lines connect corresponding points at objects. For example, to measure blackboard object dimensions, four corresponding points of A, B, C, and D must be obtained. Each corresponding point is connected to form lines: line 9, 10, 11, and 12. As described above, the survey-from-photo requires a standard scale. Therefore, the authors propose to use a ruler that is attached at an appropriate view as reference dimension in this "ruler method". A ruler is preferred because it is practical and simple to attach to the view region to be measured.

To investigate the repeatability of dimension prediction, 100 dimensions at several objects were examined. The predicted dimensions using DVP as System 2 were compared with measured dimensions obtained from laser measurements using a laser indicator (LS-501A; MAX Co., Ltd.) illustrated in Figure 4.3. The MSE and correlation coefficient (R) are applied for assessments.

4.2.3. Results of System 2

From analyses of System 2, the results are given in Figure 4.4, which revealed a high correlation coefficient ($R \geq 0.99$) between identifcation values using System 2 and measured values with $MSE \leq 0.009$. Results show that System 2 provided high reliability using no physical measurement. For detail, the comparisons in each dimension can be referred at Appendix III.

Figure 4.3.: Laser measurement equipment (LS-501A; MAX Co., Ltd.)

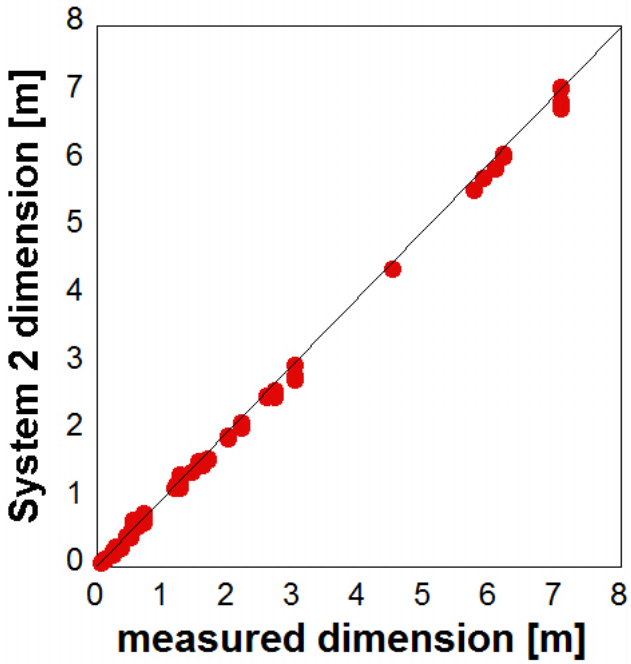

Figure 4.4.: System 2 dimensions and measured dimensions

4.3. Summary

The System 2 was performed well by using two images. This two images are used to calculate by DVP in order to measure the corresponding obejcts. A high correlations R $\geq$ 0.99 with MSE $\leq$ 0.009 is presented from System 2 which means that System 2 is able to provide high reliability in identifying object dimensions without using no physical measurement.

Chapter 5.

Development of Feed-Forward Neural Network to Estimate Reverberation Times

5.1. Introduction

The focus of this chapter is on the development of FFNN for estimating the reverberation times of a room. To investigate the reliability of FFNN estimating reverberation times, three conditions in an actual room were created. Three conditions are original condition, absorption coefficient modification on a door by attaching a tiled carpet, and absorption coefficient modification on a window by attaching a tiled carpet. Reverberation times from these three conditions using FFNN, FEA, and measured (ISO 3382) were compared.

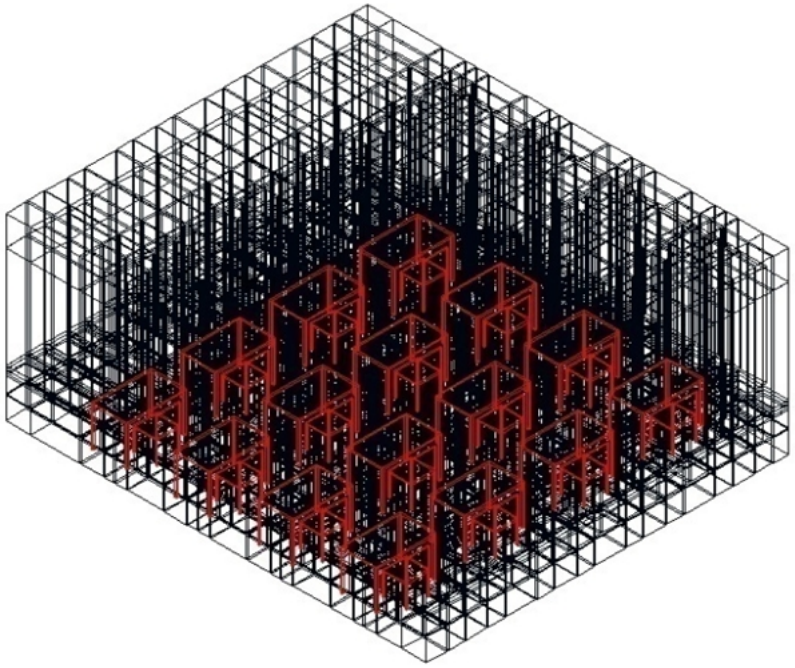

Figure 5.1.: Room mesh

Table 5.1.: FEA's Setting

No. of	overall	wall	door	floor	window	ceiling	furniture
element	60499	459	3477	3078	504	2986	5752
node	515717	520	3786	3190	570	3228	594

5.2. Methodology of Estimation Reverberation Times Using Feed Forward Neural Network

5.2.1. Source of Data

A room at Oita University was used as the model where room volume was 130.21 m^3 (7.08 m, 6.09 m, 3.02 m). Here, floor, ceiling, wall, window, door and furniture surfaces were considered as the factors to be utilized. Figure 5.1 shows the mesh of the classroom included the furniture. The mesh can be obtained by using the rule; $\lambda/d > 4.8$ (λ is acoustic wavelength, d is nodal distance) [63]. Then, Gid9 [64] computes the mesh to obtain the numbers of elements and nodes which were used in the FEA analysis as shown in Table 5.1.

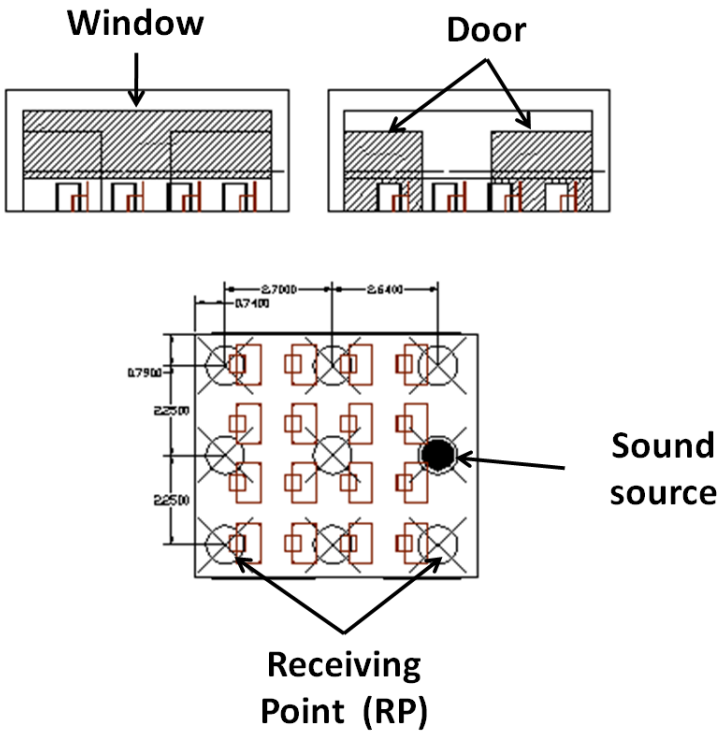

Figure 5.2.: Room layout

In the FEA, the room surfaces of absorption coefficients were employed to simulate the reverberation times. The range of the absorption coefficients of the surfaces used are floor: 0.01 - 0.2, ceiling: 0.05 - 0.88, wall: 0.02 - 0.06, window: 0.03 - 0.55, and door: 0 - 0.3. Figure 5.2 shows that the range for locations is; x axis: 0.74 - 6.08 and y axis: 0.79 - 5.29. The following equation 5.1 is expected to generate the reverberation times from the sample combination absoeptionc coefficients and receiving point locations. More than 700 sample were created.

$$RT = f_{FEA}\left[\alpha_{wall}, \alpha_{door}, \alpha_{floor}, \alpha_{window}, \alpha_{ceiling}, \alpha_{furniture}, rp_x, rp_y\right] \tag{5.1}$$

where f_{FEA} is a function of FEA. The α_{wall}, α_{door}, α_{floor}, α_{window}, $\alpha_{ceiling}$, $\alpha_{furniture}$, rp_x and rp_y is represented absorption coefficient of wall, door, floor, window, ceiling, and furniture respectively. The rp_x and rp_y is the location of receiving point

at x axis and y axis.

5.2.2. Development of Feed Forward Neural Network

Eight parameters are to be taken as a set of input parameter; α_{wall}, α_{door}, α_{floor}, α_{window}, $\alpha_{ceiling}$, $\alpha_{furniture}$, rp_x and rp_y. The combination of FFNN can be simplified as follows;

$$RT = f_{FFNN}\left[\alpha_{wall}, \alpha_{door}, \alpha_{floor}, \alpha_{window}, \alpha_{ceiling}, \alpha_{furniture}, rp_x, rp_y\right] \tag{5.2}$$

where f_{FFNN} is a function of FFNN.

Usually, before executing the training process, set of database are needed to normalize the parameters between 0.1- 0.9. The normalization can be expressed by using the equation 3.1.

More than 700 samples obtained from FEA were employed. They were divided into three subsets; train (60% of samples), validate (20% of samples) and test (20% of samples). The train subset is mostly used for computing and updating the weights and bias, the validate subset uses to monitor the training process and test subset were used to verify the performance. In addition, 35 unseen data were implemented to confirm the credibility of FFNN performance. In this case, the unseen data were an independent database which was not used for training process.

Three layers were used to build a network as shown in Figure 5.3. The input layer, which consisted of eight input neurons represents the input parameters, whereas, the ouput layer conssisted of one output neuron represents reverberation

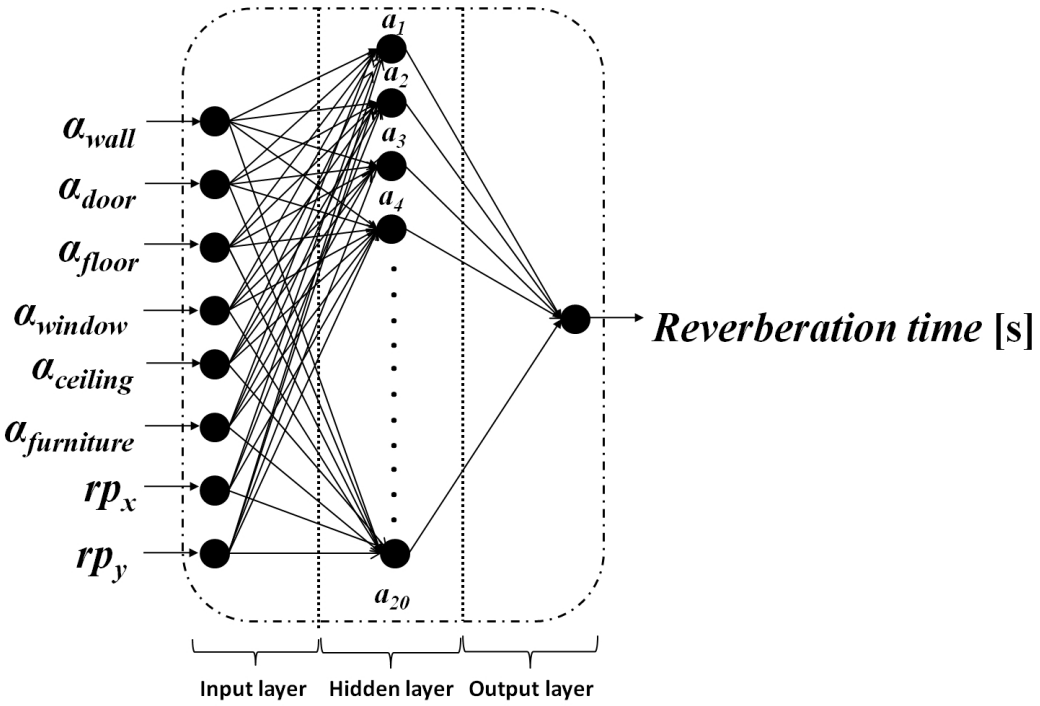

Figure 5.3.: Archiecture of FFNN for estimating reverberation times

times. Then the number of neurons in the hidden layer can be added from 2 to 15 neurons to get the optimum network architecture. Thus, a trial and error is a normal method used to identify the optimum hidden neuron which gives influence to the performance. Only one network may offer a good result. In this case the mean square error (MSE) and correlation coefficients (R) were used for the assessment.

5.2.3. Results of Feed Forward Neural Network

By referring to Table 5.2 we can observe the MSE of each subset in each hidden neuron. The optimum network of FFNN obtained from 10 hidden neurons (network architecture: [8, 10, 1]). This optimum network also performance well especially at test subset with MSE = 0.0008 with correlation coefficient R $\geq$ 0.90 which means the predicted values are close to actual values.

The unseen data were used to verify their performance. The example of

Table 5.2.: MSE of each number of hidden neuron

number of hidden neuron	MSE	
	training subset	validation subsets
2	0.0020	0.00270
3	0.00059	0.00087
4	0.00058	0.00084
5	0.00095	0.0010
6	0.00048	0.00099
7	0.00055	0.00087
8	0.00069	0.00098
9	0.00047	0.00086
10	0.00035	0.00084
11	0.00041	0.00084
12	0.00040	0.00090
13	0.00039	0.00085
14	0.00043	0.00088
15	0.00047	0.00092

unseen data are showed in Table 5.3. By using a combination of input parameters of unseen data, the FFNN was able to predict the reverberation times. Figure 5.4 illustrates the comparison of FFNN prediction between unseen data of reverberation times. The FFNN are predicted close to reverberation times unseen data with the MSE = 0.0004 with correlation coefficient R$\geq$ 0.90. Such results indicated that the FFNN yielded a good agreement in respect to unseen database of reverberation times.

5.3. Reliability of Feed Forward Neural Network

To investigate the reliability of the FFNN, three conditions at a actual room are created. These conditions can be simplified as follows;

- Condition **A**: The original condition of the room
- Condition **B**: Tiled carpet was attached to a door in the original room
- Condition **C**: Tiled carpet was a attached to a window in the original room

Table 5.3.: Unseen data

No. of unseen data	α_{wall}	α_{door}	α_{floor}	α_{window}	$\alpha_{ceiling}$	$\alpha_{furniture}$	rp_x	rp_y	RT_{FEM} unseen data
1	0.02	0.06	0.20	0.18	0.70	0.30	0.74	0.79	0.53
2	0.02	0.06	0.20	0.18	0.70	0.30	0.74	3.04	0.52
3	0.02	0.06	0.20	0.18	0.70	0.30	0.74	5.29	0.52
4	0.02	0.06	0.20	0.18	0.70	0.30	3.44	5.29	0.490
5	0.02	0.06	0.20	0.18	0.70	0.30	3.44	3.04	0.498
9	0.02	0.06	0.20	0.18	0.70	0.30	3.44	0.79	0.500
7	0.02	0.06	0.20	0.18	0.70	0.30	6.08	5.29	0.478
8	0.02	0.00	0.20	0.18	0.70	0.30	0.74	0.79	0.548
9	0.02	0.00	0.20	0.18	0.70	0.30	0.74	3.04	0.535
10	0.02	0.00	0.20	0.18	0.70	0.30	0.74	5.29	0.537
11	0.02	0.00	0.20	0.18	0.70	0.30	3.44	5.29	0.504
12	0.02	0.00	0.20	0.18	0.70	0.30	3.44	3.04	0.511
13	0.02	0.00	0.20	0.18	0.70	0.30	3.44	0.79	0.514
14	0.02	0.00	0.20	0.18	0.70	0.30	6.08	5.29	0.499
15	0.02	0.18	0.20	0.55	0.70	0.30	0.74	0.79	0.404
16	0.02	0.18	0.20	0.55	0.70	0.30	0.74	3.04	0.389
17	0.02	0.18	0.20	0.55	0.70	0.30	0.74	5.29	0.379
18	0.02	0.18	0.20	0.55	0.70	0.30	3.44	5.29	0.356
19	0.02	0.18	0.20	0.55	0.70	0.30	3.44	3.04	0.352
20	0.02	0.18	0.20	0.55	0.70	0.30	3.44	0.79	0.375
21	0.02	0.18	0.20	0.55	0.70	0.30	6.08	5.29	0.348
22	0.02	0.18	0.20	0.55	0.70	0.30	0.74	0.79	0.403
23	0.02	0.18	0.20	0.55	0.88	0.30	0.74	3.04	0.402
24	0.02	0.18	0.20	0.55	0.88	0.30	0.74	5.29	0.381
25	0.02	0.18	0.20	0.55	0.88	0.30	3.44	5.29	0.395
26	0.02	0.18	0.20	0.55	0.88	0.30	3.44	3.04	0.377
27	0.02	0.18	0.20	0.55	0.88	0.30	3.44	0.79	0.423
28	0.02	0.18	0.20	0.13	0.88	0.30	6.08	5.29	0.347
29	0.02	0.06	0.11	0.13	0.42	0.02	0.74	0.79	0.903
30	0.02	0.06	0.11	0.13	0.42	0.02	0.74	3.04	0.873
31	0.02	0.06	0.11	0.13	0.42	0.02	0.74	5.29	0.797
32	0.02	0.06	0.11	0.13	0.42	0.02	3.44	5.29	0.873
33	0.02	0.06	0.11	0.13	0.42	0.02	3.44	3.04	0.807
34	0.02	0.06	0.11	0.13	0.42	0.02	3.44	0.79	0.863
35	0.02	0.06	0.11	0.13	0.42	0.02	6.08	5.29	0.833

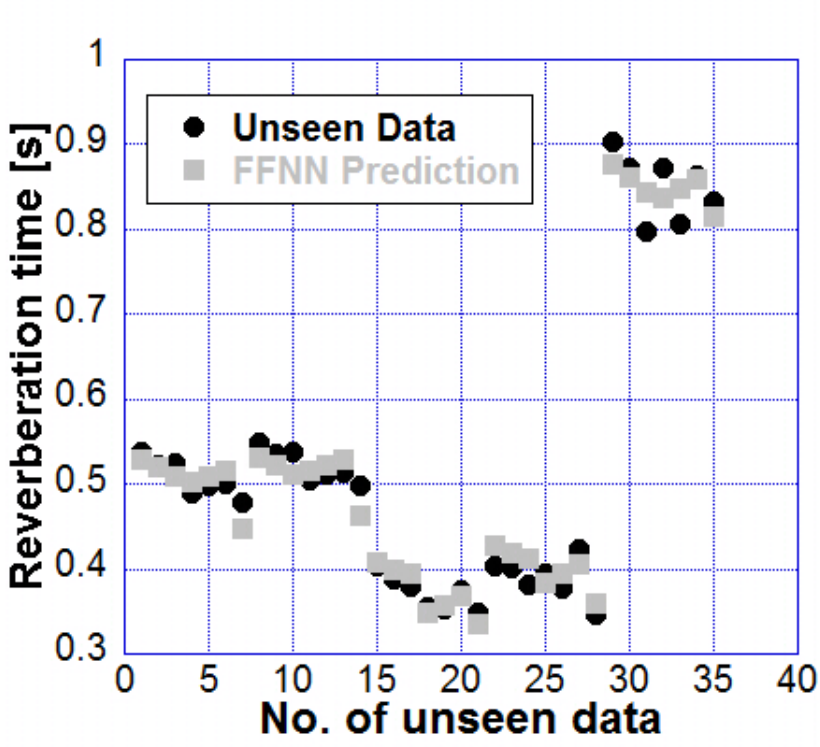

Figure 5.4.: Unseen Data Prediction

Table 5.4.: Condition setting at a room

Condition	α_{wall}	α_{door}	α_{floor}	α_{window}	$\alpha_{ceiling}$	$\alpha_{funiture}$
A	0.03	0.13	0.02	0.07	0.39	0.12
B	0.03	0.06*	0.02	0.07	0.39	0.12
C	0.06**	0.13	0.02	0.07	0.39	0.12

* tiled carpet attached on door
** tiled carpet attached on window

The absorption coefficients of material surfaces are listed in Table 5.4. Figure 5.5 illustrates the plan view of furniture layout, location of receiving points and location of sound source in a room.

The parameters given in Table 5.4 were fed into FFNN to estimate the reverberation times at each receiving points. Subsequently, a series of measurement is conducted in three conditions of a room to obtain the reverberation times following ISO 3382-2:2008 [18]. Figure 5.6 (a), (b) and (c) show the measurement conditions in a room. In addition, simulated results of FEA were also provided to compare them with results by FFNN and measurements.

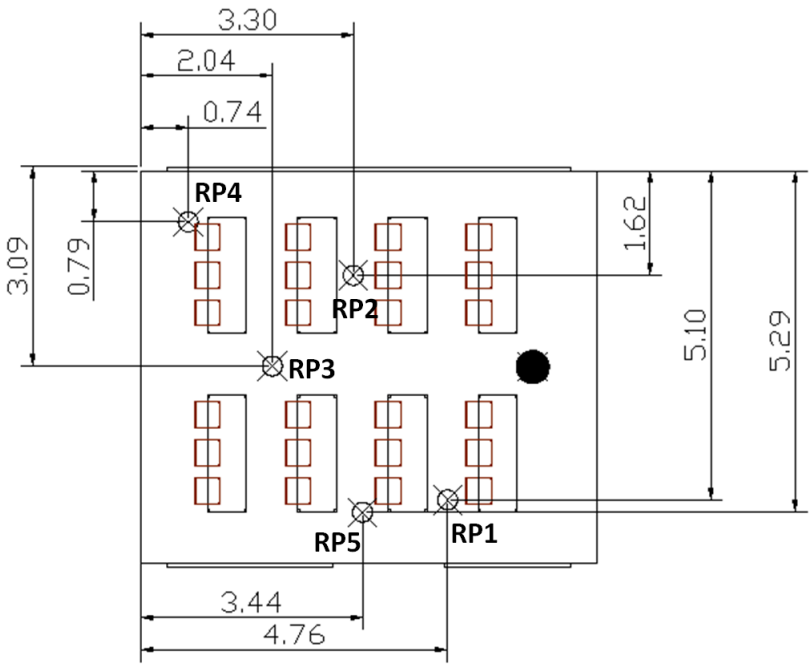

Figure 5.5.: Location of receiving points

Figure 5.7 presents the comparisons of reverberation times at each receiving points between estimated results by FFNN, simulated results by FEA and measured results. Here, the MSE between measured results and FFNN was more than 0.002, while MSE between measured results and FEA was more than 0.005. This indicated the that predicted FFNN approximates to measured data rather that FEA. The reason for this is that the consistence of FFNN prediction located closer to measured data, whereas the FEA was unstable especially at Condition B and C in RP2 and RP3.

In general, the FEA computing time is around few hours. Therefore, this study develops a FFNN model as a option for estimating the reverberation times with 1 s. The FFNN is user friendly and can be used at preliminary stages either for constructing or for renovating rooms with acceptable reverberation times.

(a) Condition A

(b) Condition B

(c) Condition C

Figure 5.6.: Three type of conditions of a room

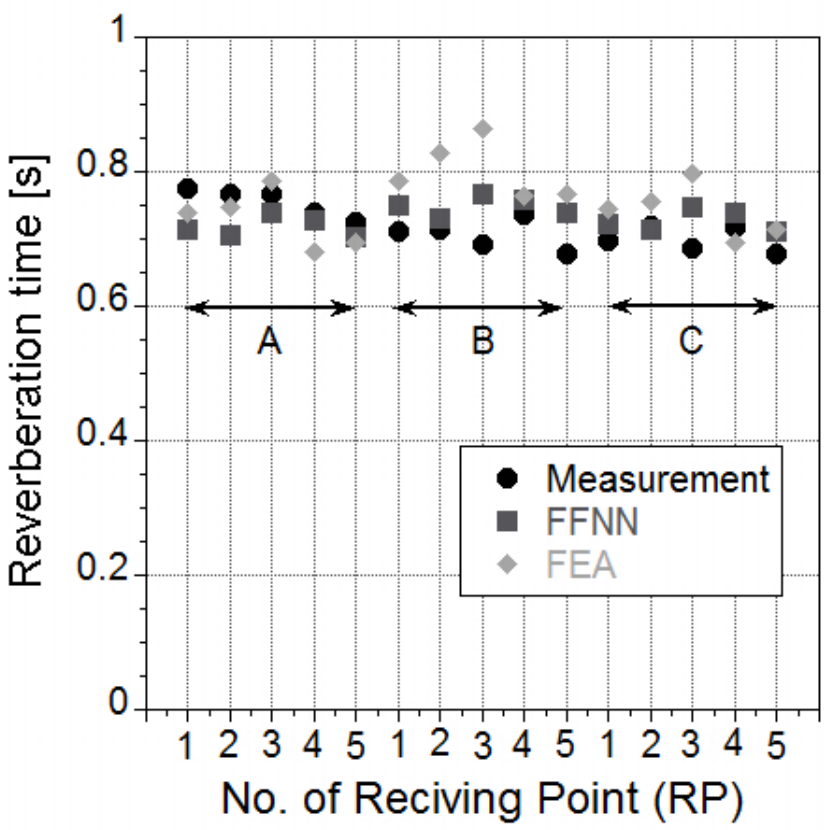

Figure 5.7.: Comparison of FFNN, FEA and measurement

5.4. Summary

A technique for estimating on reverberation times using FFNN in a room is presented. In this work, the capability on FFNN estimated in variety of absorption coefficients show a good agreement with measured values. By using three conditions (condition A, B and C), the comparison between FFNN and measured results produced acceptable results with the MSE ≥ 0.002. The estimations are obtained within 1 s.

Chapter 6.

Implementation of System 1 and System 2 in Actual Rooms to Simulate Reverberation Times Using Feed Forward Neural Network and Finite Element Analysis

6.1. Introduction

The purpose of this chapter is to investigate the reliability of System 1 and System 2 on actual rooms. The estimation form both systems were used to simulate the reverberation times using FFNN and FEA. The FFNN and FEA were compared to identify the capability of the simulation of reverberation times.

6.2. Feed Forward Neural Network Implementation

6.2.1. Source of Data

As a forementioned, the FFNN required database for training process. The author used eight simulation rooms and five types of furniture as illustrated in Figure 6.1 and Figure 6.2. By random combinations of rooms and furniture, about 20 rooms were obtained. These rooms were simulated using FEA to obtain the reverberation times. In this simulation, six absorption coefficients of material surfaces wall, door, floor, window, ceiling and furniture were considered at this stage. Basically, the absorption coeficient values (ranging 0 to 1) depend on the type of material either reflective of absorptive. To consider all the absorption coefficient values, it is necessary to increase computing times; however, this increases the cost of FEA. To overcome the problem, two kinds of conditions were considered;

1. dead: $\alpha_{wall} = 0.08$, $\alpha_{door} = 0.1$, $\alpha_{floor} = 0.06$, $\alpha_{window} = 0.4$, $\alpha_{ceiling} = 0.4$, $\alpha_{furniture} = 0.4$

2. live: $\alpha_{wall} = 0.02$, $\alpha_{door} = 0.02$, $\alpha_{floor} = 0.02$, $\alpha_{window} = 0.04$, $\alpha_{ceiling} = 0.2$, $\alpha_{furniture} = 0.4$

Dead is the maximum value of absorption coefficient, whereas live is the minimum value of absorption coefficient. These conditions were obtained from several material surfaces at Oita University's rooms. The following equation 6.1 is expected to generate the reverberation times. 1220 databases of reverberation times were created.

$$RT = f_{FEA}[\alpha_{wall}, \alpha_{door}, \alpha_{floor}, \alpha_{window}, \alpha_{ceiling}, \alpha_{furniture}, S_{wall}, S_{door}, ...$$

$$....S_{floor}, S_{window}, S_{ceiling}, S_{funiture}, X, Y, Z, rp_x, rp_y] \quad (6.1)$$

where, S is surface area of material, X, Y, and Z is room dimension, respectively for x axis, y axis and z axis.

6.2.2. Development of Feed Forward Neural Network

Database of 1220 reverberation times obtained form 20 simulated rooms by FEA were fed into FFNN. Database is needed to normalize between 0.1 - 0.9. The normalization can be expressed using the equation 3.1. The database was divided into two subsets which are training subset and validation subset. The propotions of the subsets are 70% of databases for training subset and 30% of databases for validate subsets. To develop the architecture of FFNN, 17 parameters are to be taken as a set of input parameter of FFNN and one output parameter. The function of FFNN can be simplified as follows;

$$RT = f_{FFNN}[\alpha_{wall}, \alpha_{door}, \alpha_{floor}, \alpha_{window}, \alpha_{ceiling}, \alpha_{furniture}, S_{wall}, S_{door}, ...$$

$$....S_{floor}, S_{window}, S_{ceiling}, S_{furniture}, X, Y, Z, rp_x, rp_y] \quad (6.2)$$

To comfirm the reliability of the estimation, 360 unseen data of reverberation times were obtained from six simulated rooms.

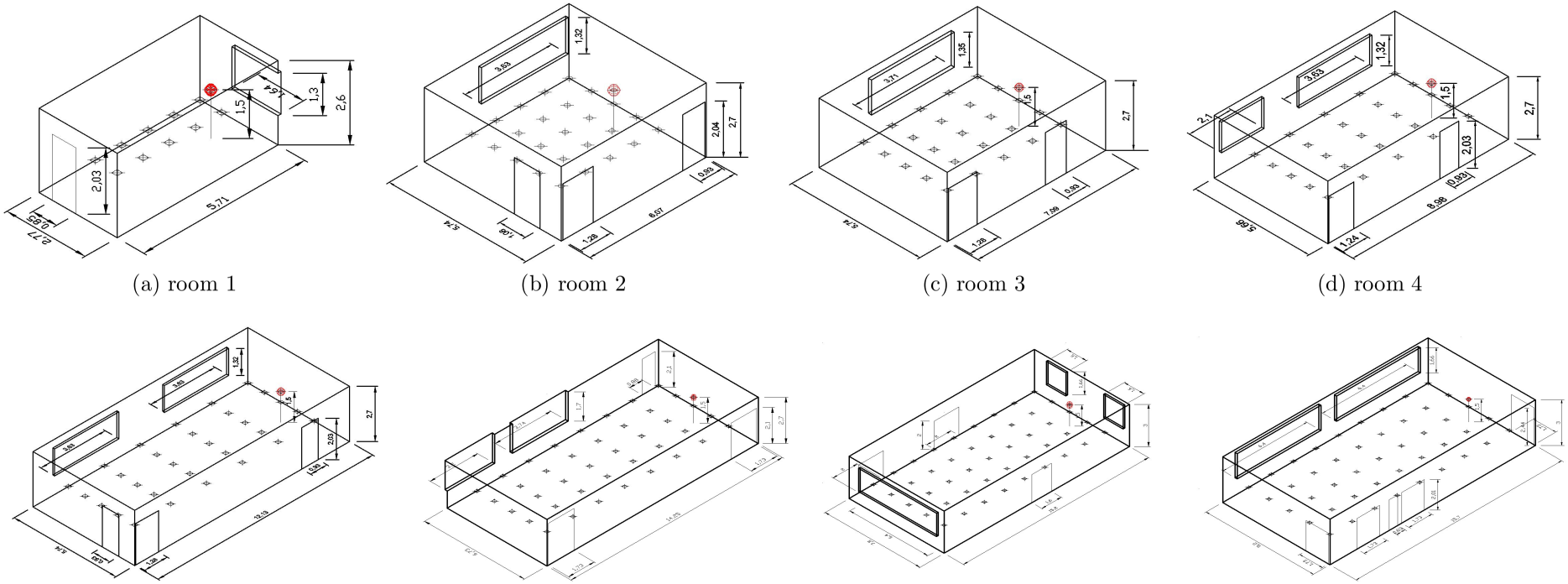

(a) room 1 (b) room 2 (c) room 3 (d) room 4

(e) room 5 (f) room 6 (g) room 7 (h) room 8

Figure 6.1.: Schematic drawing of the 8 rooms for FFNN learning database

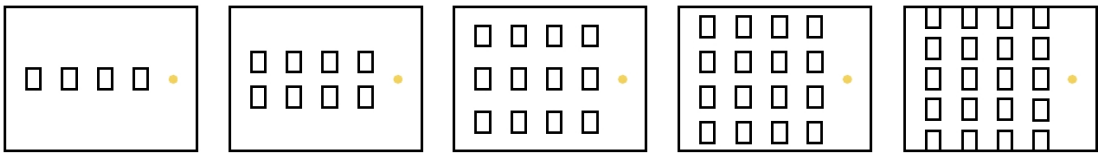

Figure 6.2.: Five types of number of furniture

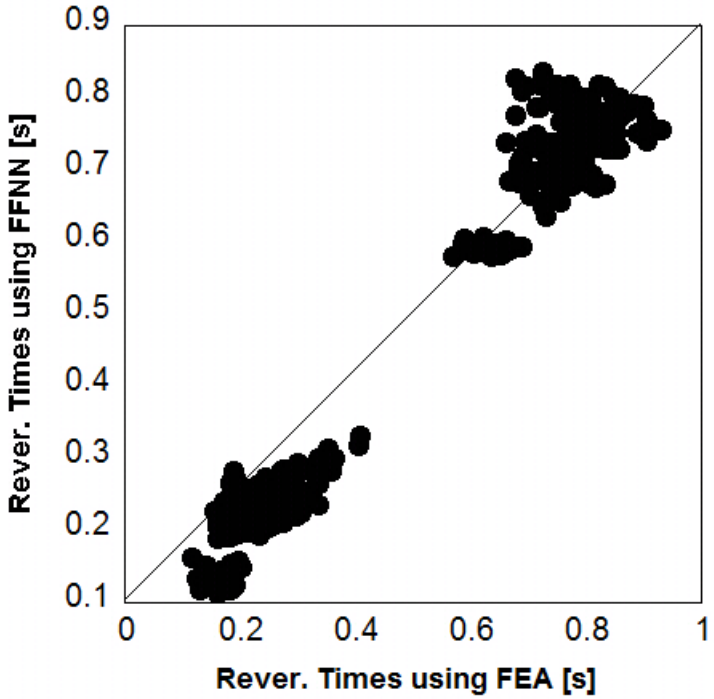

Figure 6.3.: Comparison of reverberation times between FFNN and FEA

6.2.3. Performance of Feed Forward Neural Network

From the analysis, the optimum network is [4,11,1] with training and validation subsets indicate MSE $\leq$ 0.001 with the correlation coefficient R $\geq$ 0.9 for both subsets. To comfirm the performance of reverberation times estimation, the unseen databases were used. A comparison between FFNN and FEA indicated MSE $\leq$ 0.007 and correlation coefficient R $\geq$ 0.8 (Refer. Figure 6.3). At this stage, the FFNN was useful for estimating the reverberation times of rooms. Results yielded a good reliability for the estimation of reverberation times on the unseen databases.

6.3. Implementation in Actual Rooms

6.3.1. Actual Rooms Descriptions

Here, two types of rooms with different volumes (130 m^3 and 260 m^3) taken from Oita University were used. Normally, a room contains of number of pieces of furniture (desks and chairs). Thus, the furniture was added to investigate the effects of reverberation times between measurements and estimates using System 2.

For the analysis, in each room we added two types of furniture. Type 1: Room 1 and Room 2 have 130 m^3, Type 2: Room 3 and Room 4 have 260 m^3. Room 1 was added simulations furniture and Room 2 was added from measured furniture as shown in Figure 6.4 (a) and (b), respectively. Room 3 was empty room and Room 4 was added from the measured furniture as shown in Figure 6.4 (c) and (d), respectively. The description of dimensions of rooms can be referred to in Table 6.1.

The measured furniture was measured from one desk and one chair. Then, each desk and chair were combined and increasing the number of number Referring to Figure 6.5 that we used for analysis, the desk and chair seemed to have a complicated design which made it difficult to measure the dimensions especially using System 2. Therefore, in this case, the author only considered the important dimensions of the desk and chair. The important dimensions are shown in Figure 6.6 (a), (c) and (e). Thus, the desk and the chair were designed by following simulation funiture. Figure 6.6 (b), (d) and (f) show a schematic drawing for a desk and a chair that were used for the next analysis.

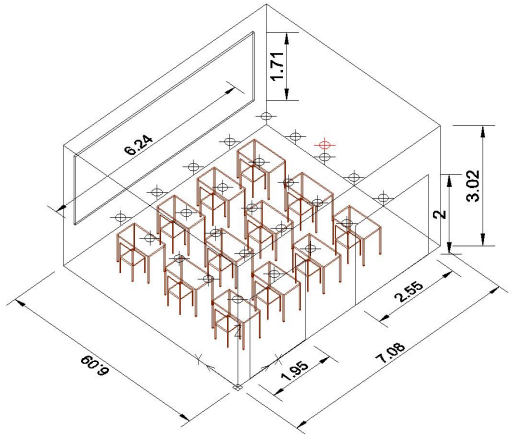

(a) Room 1

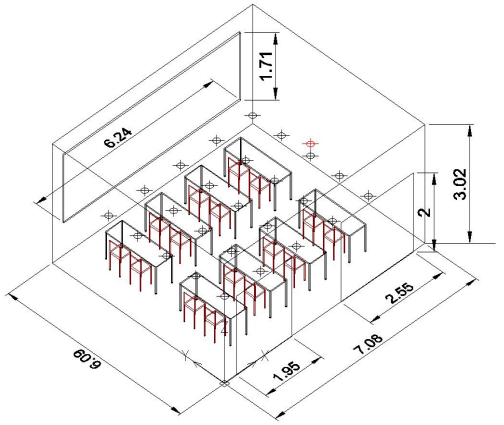

(b) Room 2

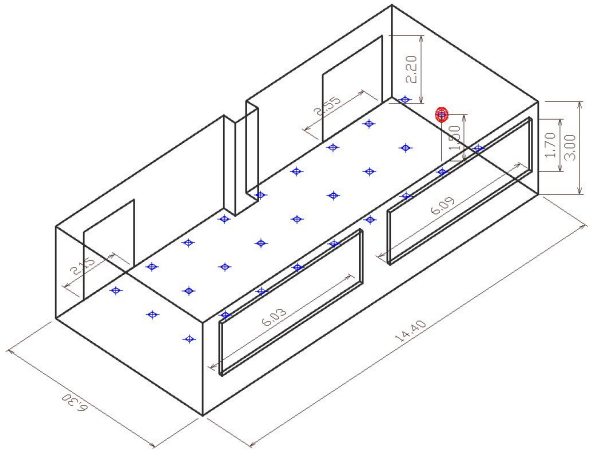

(c) Room 3

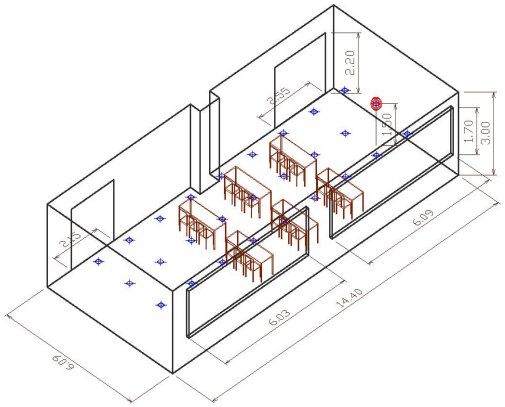

(d) Room 4

Figure 6.4.: Four types of rooms

Table 6.1.: Dimension description of rooms

Type of room	room axis			door 1		door 2		window 1		window 2		furniture
	axis (m)			axis (m)		axis (m)		axis (m)		axis (m)		total area
	x	y	z	x	y	x	y	x	y	x	y	(m^2)
1	7.08	6.09	3.02	1.95	2.00	2.55	2.00	6.24	1.71	x	x	25.14
2	7.08	6.09	3.02	1.95	2.00	2.55	2.00	6.24	1.71	x	x	32.14
3	14.18	6.11	3.00	2.15	2.20	2.55	2.20	6.03	1.7	6.09	1.7	empty
4	14.18	6.11	3.00	2.15	2.20	2.55	2.20	6.03	1.7	6.09	1.7	28.71

(a)

(b)

(c)

Figure 6.5.: Types of furniture

(a)

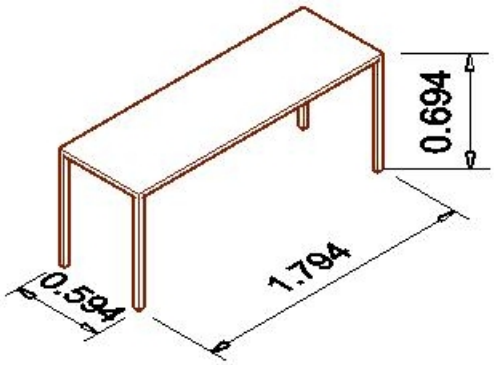

(b)

(c)

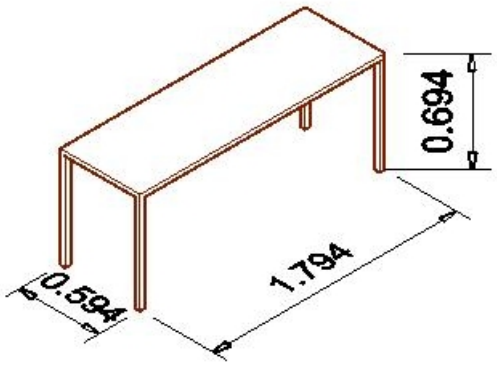

(d)

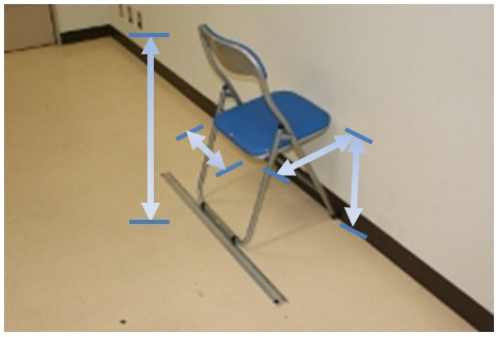

(e)

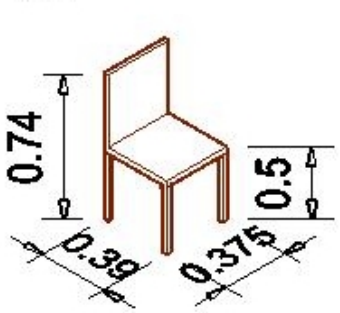

(f)

Figure 6.6.: Important dimensions and schematic drawing of funiture

6.4. System 1 Implementation

For System 1, 294 images of material surfaces were obtained (surface (a) = 60 images, surface (b) = 53 images, surface (c) = 48 images, surface (d) = 63 images, surface (e) = 41 images, and surface (f) = 25 images). A limitation $(\bar{x} - \sigma)$ and $(\bar{x} + \sigma)$ of coefficient values for all images was calculated by using the procedures described above. Surfaces consisting of coefficient values within the limit were used to feed into FFNN.

Based on this limitation, there are 61% from 294 images (surface (a) = 32 images, surface (b) = 35 images, surface (c) = 33 images, surface (d) = 31 images, surface (e) = 26 images and surface (f) = 23 images). Images of surface materials that consist of coefficient values within the limitation were fed into FFNN. Figure 6.7 shows the limitation of four coefficient values for the six surface images that were used for FFNN.

6.4.1. Results and Discussions

Figure 6.8 reveals that prediction by System 1 yields a good correlation coefficient R $\geq$ 0.90. Unfortunately, estimations on 3 Surface (d) (α = 0.04) showed inconsistent results because 29% of 31 surface images were below the limit at ASM training surface image database as shown in Figure 6.9. The window is a transparent and has a light-reflecting material. In this case of a transparent window, it is difficult to capture consistent images of material surfaces because of their surface characteristics.

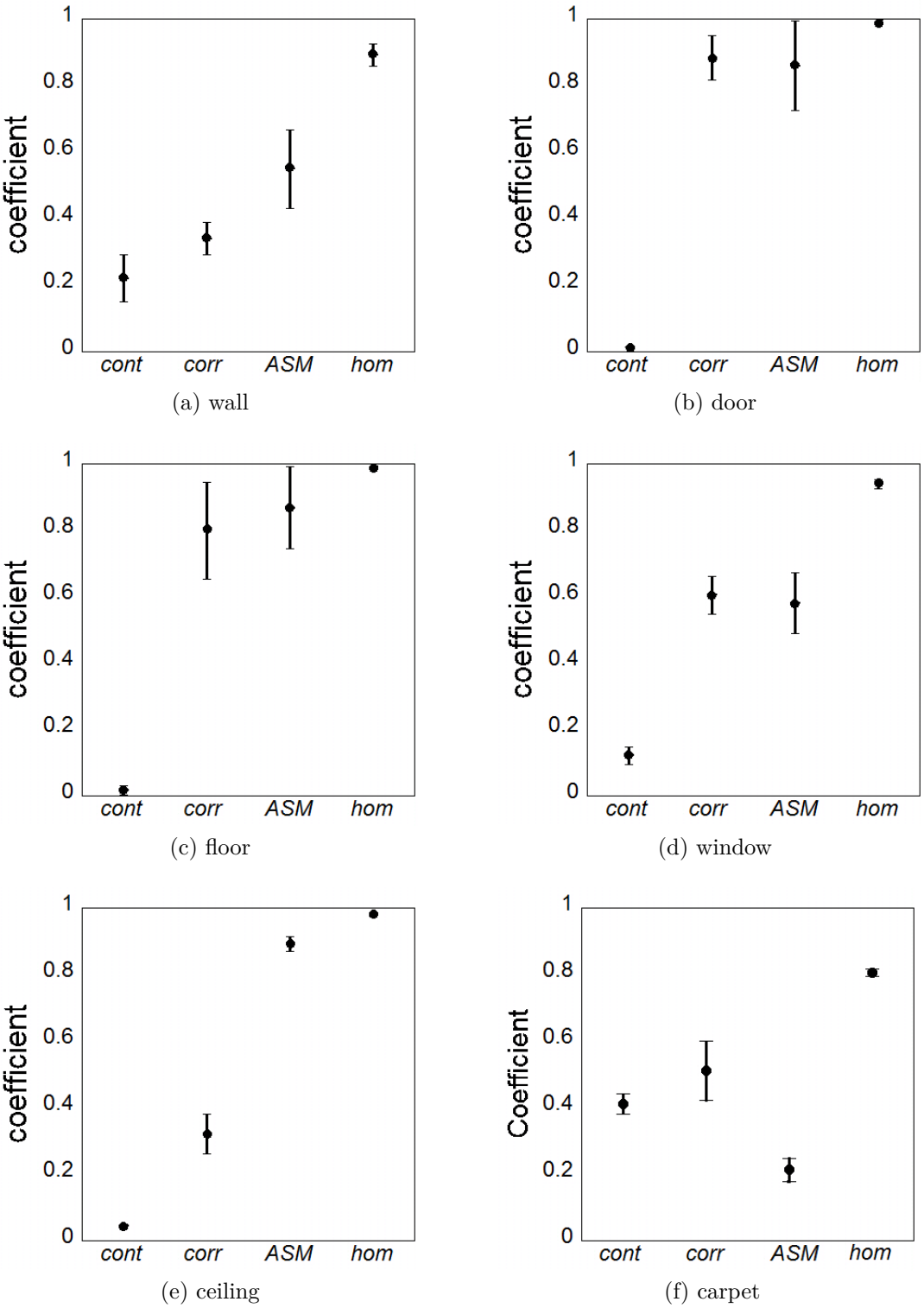

(a) wall (b) door

(c) floor (d) window

(e) ceiling (f) carpet

Figure 6.7.: Limitation of coefficient values for six surface images

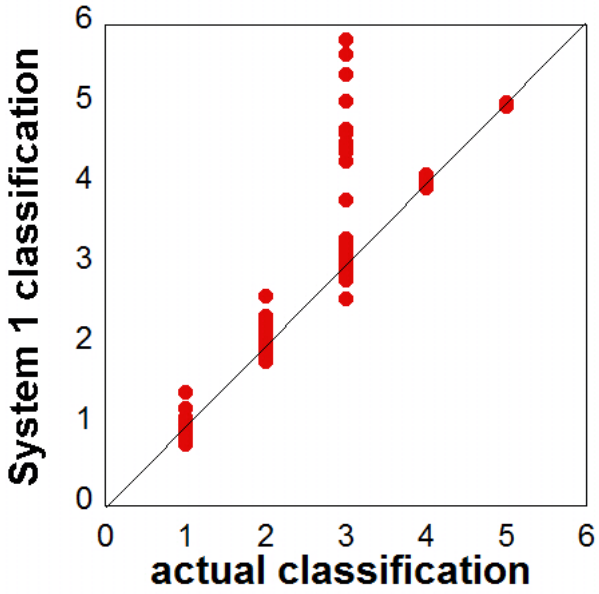

Figure 6.8.: System 1 and actual classification in actual rooms

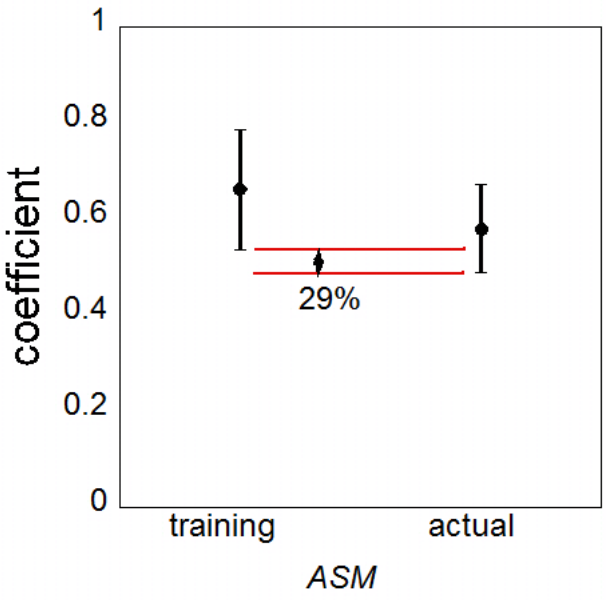

Figure 6.9.: Comparison limitation of ASM between training and actual for window

6.5. System 2 Implementation

At System 2, the target objects were the wall, floor, ceiling, door, window, and furniture. These objects were captured by using a camera and fed into DVP to identify the dimensions. The same procedure (ruler method) as explained in subchapter 4.2 were employed. Figure 6.10 and Figure 6.11 show an example of two rooms that were used to measure the objects. The main part was the corresponding points located at the objects and in the line connection line between two corresponding points.

6.5.1. Results and Discussions

Figure 6.12 illustrates the estimation results of room dimensions. Following the capture procedure, the System 2 yeilds high correlation coefficient R $\geq$ 0.99 with MSE $\leq$ 0.200 in estimating the dimensions. Figure 6.13 and Figure 6.14 show a comparison of schematic drawing between measured dimensions and System 2 estimations.

6.6. Reverberation Times Estimation Using Feed Forward Neural Network and Finite Element Analysis

To estimate the reverberation times, the FFNN and FEA use same input parameters obtained from System 1 and System 2. Referring to the results of System 1, window surface shows inconsistent results. The reason for this is that at this stage it was necessary to investigate the reliability of estimation reverberation times using FFNN and FEA. Therefore, the author used the actual classification numbers.

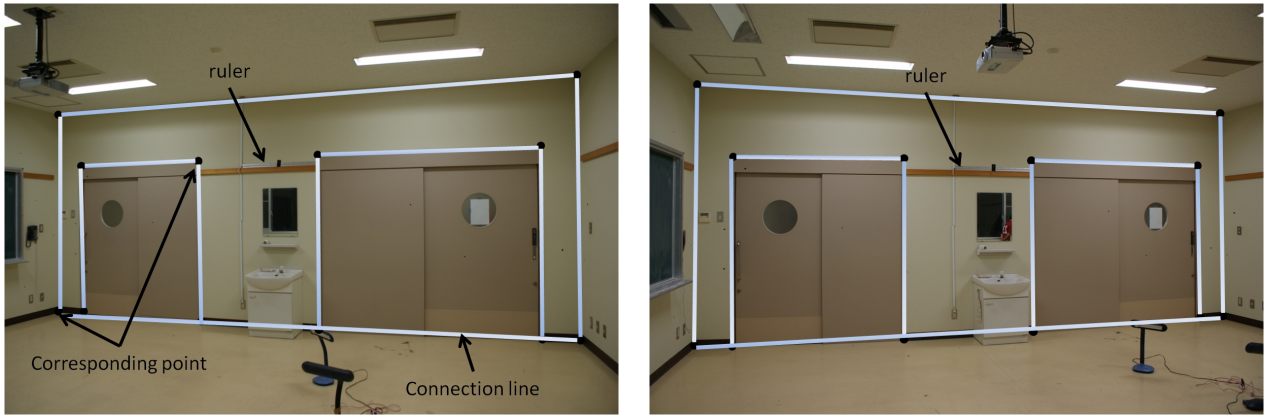

(a) (b)

Figure 6.10.: Room with volume = 130m^3

(a) (b)

Figure 6.11.: Room with volume = 260m^3

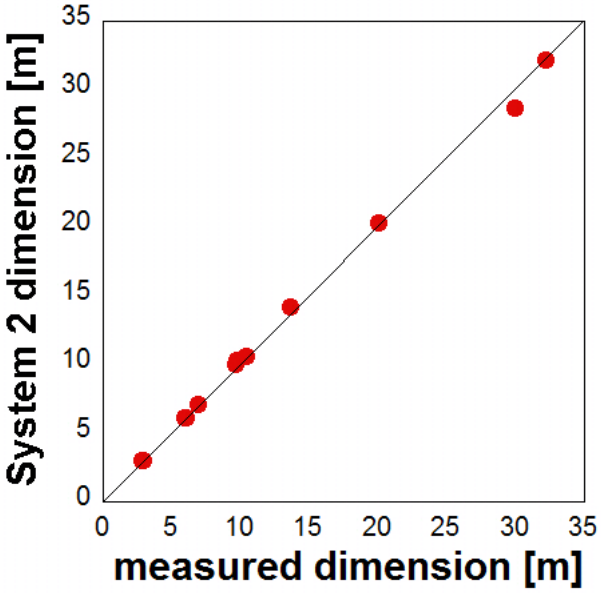

Figure 6.12.: System 2 dimensions and measured dimensions for actual rooms

As mentioned previously, System 1, the classification numbers represents the type of material surfaces. At the same time, the absorption coeffiicents were also obtained as shown in Table 3.3. However, the simulation of rooms were included the furniture. In this case, the absorption ceofficient of the funiture of 0.4 was used.

System 2 are obtained the dimension of rooms. To obtain the reverberation times, the receiving points were set at certain locations in a room. Two rooms (Room 1 and Room 2) were set with 25 receiving points each. The other two (Room 3 and Room 4) were set with 27 receiving points each. The totals of receiving points of the four rooms were 104.

6.6.1. Results and Discussions

Reverberation times were obtained by FEA using the parameters from System 1 and System 2 (RT_{FEA} system) are compared with reverberation times obtained by FFNN using parameters from System 1 and System 2 (RT_{FFNN} system). The results indicate correlation coefficients $R \geq 0.3$ shown in Figure 6.15.

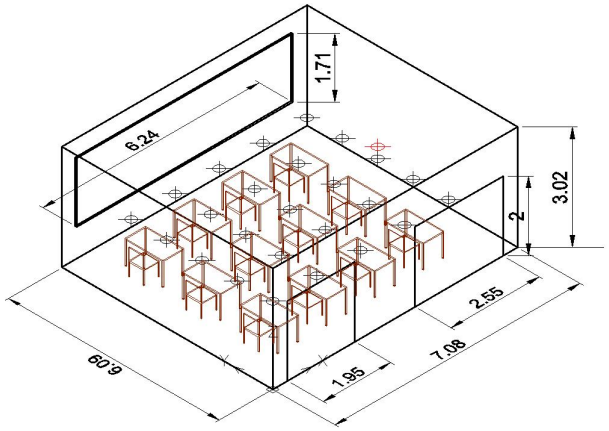

(a) Room 1 for measured values

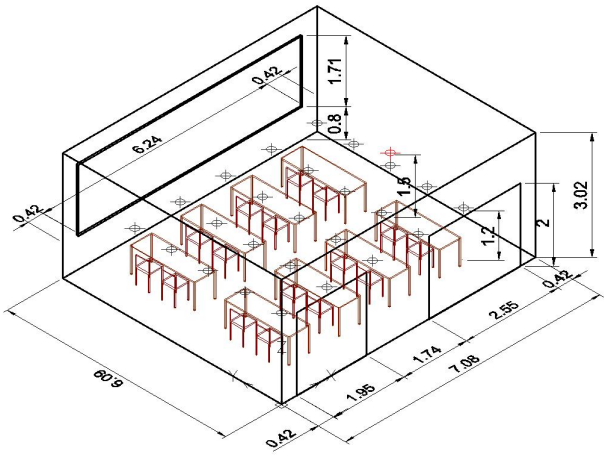

(b) Room 2 for measured values

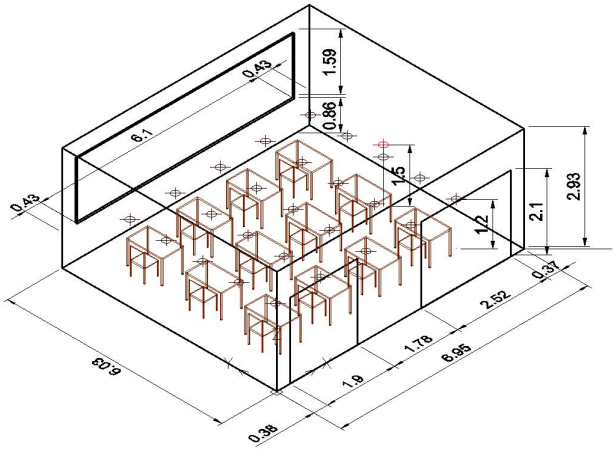

(c) Room 1 for System 2

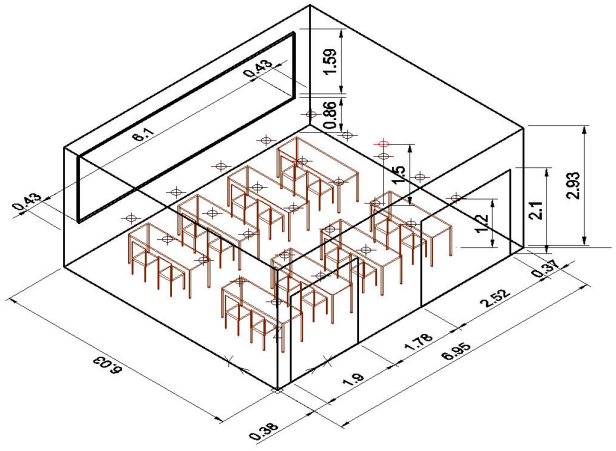

(d) Room 2 for System 2

Figure 6.13.: Schematic drawing between measured dimensions and System 2 for Room 1 and Room 2

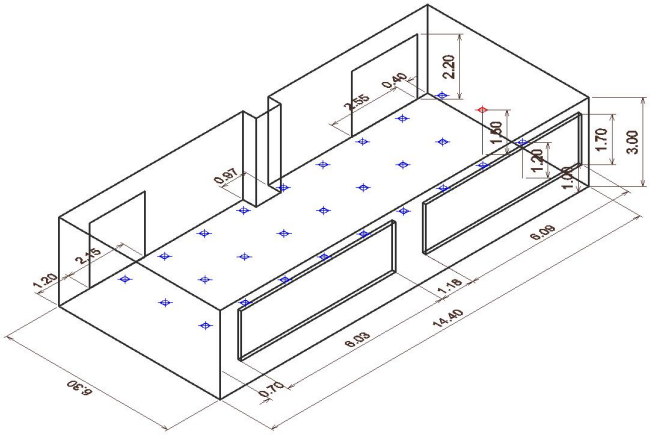

(a) Room 3 for measured dimensions

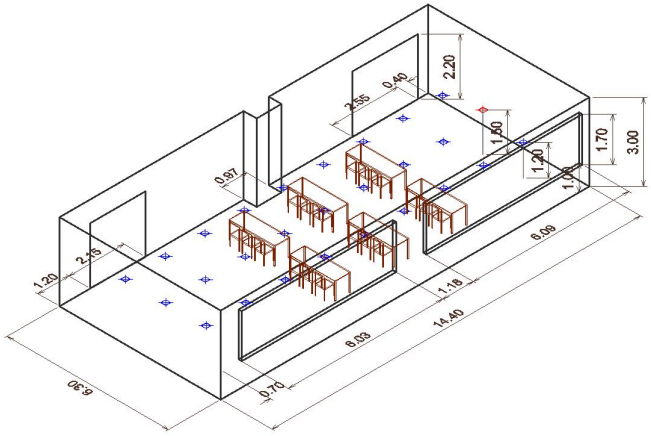

(b) Room 4 for measured dimensions

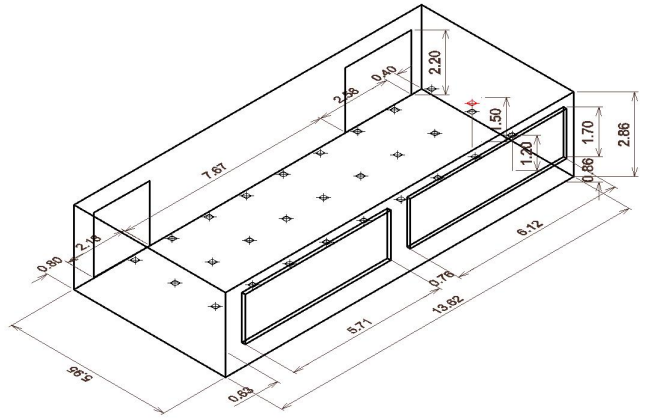

(c) Room 3 for System 2

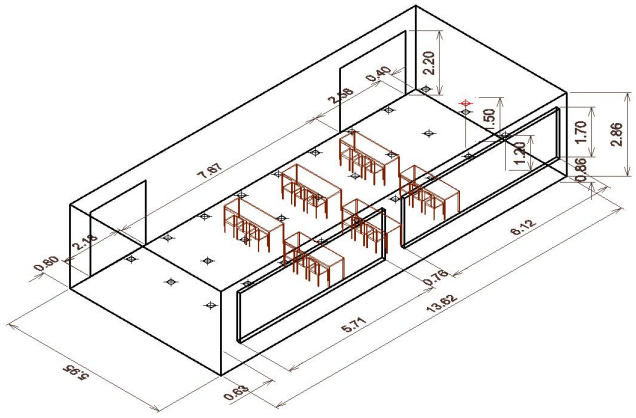

(d) Room 4 for System 2

Figure 6.14.: Schematic drawing between measured dimensions and System 2 for Room 3 and Room 4

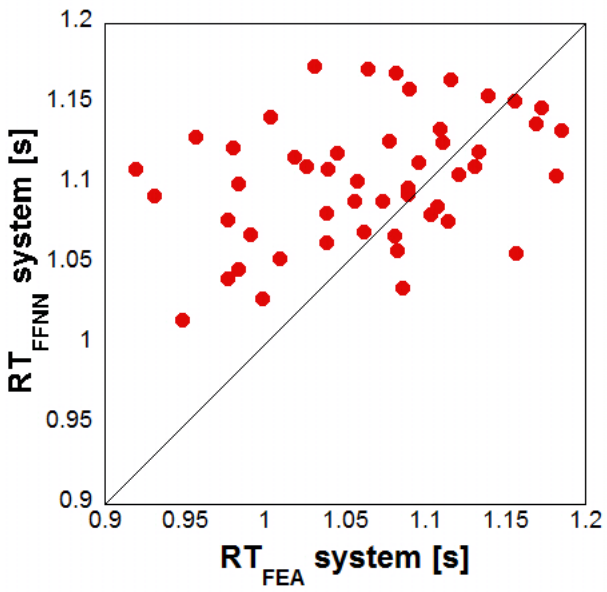

Figure 6.15.: Comparison between RT_{FFNN} system and RT_{FEA} system for actual rooms

However, reverberation times obtained by FEA using parameters obtained from systems System 1 and System 2 (RT_{FEA} system) are compared with RTs by FEA using actual absorption coefficients and dimensions (RT_{FEA} actual) in Figure 6.16. This process yielded practical results of reverberation times at 104 receiving points with correlation coefficient $R \geq 0.85$ and MSE ≤ 0.008, which means that the reverberation times can be simulated well by FEA using both systems.

Results revealed that the techniques of Systems 1 and 2 provide good identification capability to actual rooms and at this stage both are also useful to simulate the reverberation times of rooms using FEA.

6.7. Summary

The above mentioned results indicate that System 1 and 2 are able to identify the material surfaces and dimensions of rooms. The reliability of both systems were confirmed in actual rooms with the correlation coefficient $R \geq 0.90$, and we employed their identifications to simulate reverberation times of the

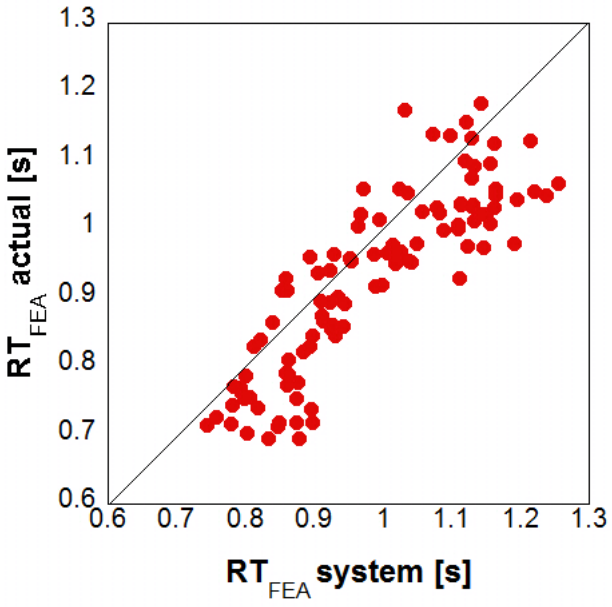

Figure 6.16.: Comparison between RT_{FEA} actual and RT_{FEA} system for actual rooms

rooms using FEA. FEA is one of the computation technique used for simulating rooms sound field. The System 1 and System 2 show potential for use in other techniques e.g. ray-tracing, FEA, BEA Sabine and Eyring. FFNN is also can be used for estimating the reverberation times [65]. However, further investigation is necessary to imporve the performance of estimations.

Chapter 7.

Conclusion

7.1. Summary

The aim of this research was to develop systems for identifying material surfaces and estimating room dimensions by using photographic images. System 1, using GLCM, was adopted to analyze the texture features of image of material surfaces. The Haralick coefficients were fed into FFNN to identify the surface material. Simultaneously, the absorption coefficient is obtainable. System 2, comprising DVP and the "ruler method", was used to identify the dimensions of rooms.

System 1 in Chapter 3; six material surfaces were used to develop the system that can identify the material surfaces. To identify such material surfaces two techniques were implemented known as; i. Gray Level Co-occurrence Matrix with Haralikc coefficients ii. Feed Forward Neural Network. The GLCM function is to extract the image into statistical approach. It is difficult to implement directly. Therefore, four Haralick's coefficients were used as follows; i. contrast, ii. correlation, iii. angular second moment, and iv. homogeneity. The four of

Haralick coefficients are coefficients values of material surface images. The FFNN identified the material surfaces based on the coefficient values. Simultaneously, the absorption coefficients were obtainable.

The six material surfaces were captured by using an ordinary camera. The images material surfaces were analyzed using GLCM with Haralick's coefficients. However, the range of each material surface obtained wide range. It occurred because of the variation of brightness and texture fixtures. To solve this problem, a limitation for each coefficient values was made using means (x) and standard deviations (σ). After the limitations, material surfaces of door and floor obtained approximately similar coefficient values. To avoid redundancy during the FFNN learning process, both were integrated into the same surface image.

The results revealed a correlation coefficient $R \geq 0.90$ with $MSE \leq 0.0018$ on training and validation classifications. To confirm the performance of estimating material surfaces, this study used 36 images as testing subset. Finding showed the correlation coefficient $R \geq 0.90$ with $MSE \leq 0.0075$. At this stage, the performance of System 1 performed efficiently.

System 2 in Chapter 3; DVP was used to develop the system that can be estimated the dimensions. This system implemented "stereo vision principle", which used two images captured from different positions. The object to be measured should be viewed at both images. The object was marked with two corresponding points. Then both corresponding points were connected by a line that was used to measure the object dimension. Typically, both images comprised different scales. To standardize the scale, the author proposed "ruler method"

To examine the repeatability of System 2, 100 dimensions at several objects were examined. From analyses, the results revealed a high correlation coefficient $R \geq 0.90$ with $MSE \leq 0.009$ between estimating values using System

2 and measured values using laser measurement. At this stage, System 2 yielded high reliability using no physical measurements.

The development of FFNN for estimating reverberation times in Chapter 4. FFNN was used to investigate the reliability for estimating the reverberation times. FFNN requires learning database. Thus, FEA was employed to create reverberation time's database for FFNN learning process. A room at Oita University was used to obtain the reverberation times. The room surfaces of absorption coefficients are used to simulate the reverberation times. The ranging of the absorption coefficients of the surfaces used were floor: 0.01 - 0.2, ceiling: 0.05 - 0.88, wall: 0.02 - 0.06, window: 0.03 - 0.55, and door: 0 - 0.3. More than 700 reverberation times database has been created.

The results of experiments indicated that the training subset obtained MSE $\leq$ 0.0004 with R $\geq$ 0.90 and the validation subset obtained MSE $\leq$ 0.0009 with R $\geq$ 0.90. While, testing subset obtained with MSE = 0.0008 with correlation coefficient R $\geq$ 0.98. To verify the performance of estimations, unseen data was employed. FFNN showed a good agreement with MSE = 0.0004 and correlation coefficient R $\geq$ 0.90.

Three conditions in an actual room were created to investigate the reliability of FFNN in estimating reverberation times. The three conditions were as follows;

1. original condition,

2. attaching tiled carpet to a door, and

3. attaching tiled carpet to a window.

The FFNN estimations of reverberation times were compared with the estimation of reverberation times by FEA and reverberation times by

measurement. The analyses showed that the estimation of reverberation times using FFNN was closer to the measured reverberation times with MSE = 0.002. At the stage, the capability on FFNN estimated in variety of absorption coefficients showed a good agreement with measured values.

The implementation of System 1 and System 2 to simulate reverberation times was carried out in two roms at Oita University with different volumes (130 m^3 and 260 m^3). Then, the different types of furniture were added in each room. By adding some furniture, four rooms were created.

System 1 yielded good correlation coefficient $R \geq 0.90$. However, window surface showed inconsistent results because 29% of coefficient values of ASM for actual rooms waas below the limit for coefficient values of ASM for FFNN learning database. It was difficult to capture consistent window surface images because of surface characteristics such as transparent and light-reflecting material. System 2 revealed a high correlation coefficient $R \geq 0.90$ with MSE ≤ 0.2.

The identification parameters from System 1 and System 2 were used to simulate rooms' reverberation times by FEA and FFNN. Comparison between FEA using estimation parameters from System 1 and System 2 (RT_{FEA} system) with FFNN using estimation parameters form System 1 and System 2 (RT_{FFNN} system) indicated correlation coefficient $R \geq 0.3$. While, comparison between FEA using estimation parameters from System 1 and System 2 (RT_{FEA} system) with FEA using actual parameters (RT_{FEA} actual) yielded $R \geq 0.85$ with MSE ≤ 0.008.

Practical systems to identify the material surfaces and to estimate room dimensions are developed. System 1 is used to identify the material surfaces and simultaneous the absorption coefficients are obtained. System 2 is used to estimate the dimensions of rooms. Both of these systems provided good estimations of performance.

The estimations of room reverberation times using FFNN are developed. The FFNN is user-friendly and can estimate the reverberation times within 1 s. The results yielded that FFNN obtained acceptable reverberation times' estimations by comparing them with actual reverberation times.

The estimations from System 1 and System 2 were applied to FFNN and FEA to estimate the reverberation times of rooms. Then, the reverberation times' estimate by FFNN were compared to the reverberation times' estimated by FEA and reverberation times estimated by FEA were compared with the reverberation times estimated by FEA using actual pamateter. The comparison results yielded reverberation times estimated by FEA showed significant results between reverberation times estimated by FEA using actual pamateter

7.2. Recommendation for Future Studies

More work is still necessary to enhance the efficiency and applicability. The following works are suggested:

1. Adding more the Haralick coefficients to enhance the accuracy of surface material estimations.

2. Improving the capturing technique to estimate the dimensions precisely and simulate rooms in 3D modeling.

3. Adding more simulation rooms and combinations of absorption coefficients for FFNN learning process to increas the capability of estimation reverberation times.

References

[1] W. C. Sabine. *Collected paper on acoustic (1900)*. Dover, New York, 1964.

[2] C. F. Eyring. Reverberation time in "dead" rooms. *Journal of Acoustical Society of America*, 1:271–241, 1930.

[3] G. Millington. A modified formula for reverberation. *Journal of Acoustical Society of America*, 4:69–82, 1932.

[4] D. Fitzroy. Reverberation formula which seems to be more accurate with nonuniform distribution of absorption. *Journal of Acoustical Society of America*, 7(31):893–897, 1959.

[5] M. Hodgson. Empirical prediction of speech levels and reverberation in classrooms. *Building Acoustics*, 8:1–14, 2001.

[6] M. Hodgson and G. Wong. Ray-tracing prediction of optimal conditions for speech in realistic classrooms. *Applied Acoustics*, 70:915–920, 2009.

[7] Z. Xiangyang, C. Ke'an, and S. Jincai. On the accuracy of the ray-tracing algorithms based on various sound receiver models. *Applied Acoustics*, 70:915–920, 2003.

[8] T. Okuzono, T. Otsuru, R. Tomiku, and N. Okamoto. Fundamental accuracy of time domain finite element method for sound field analysis of rooms. *Applied Acoustics*, 71:940–946, 2010.

[9] R. Tomiku, T. Otsuru, and Y. Takahashi. Finite element sound field analysis of diffuseness in reverberation rooms. *Journal of Asian Architecture and building engineering*, 1(2):33–39, 2002.

[10] S. Kopuz and N. Lalor. Analysis of interior acoustic fields using the finite element method and the boundary element method. *Applied Acoustics*, 45:193–210, 1995.

[11] A. Tadeu and P. Santos. Assessing the effect of a barrier between two rooms subjected to low frequency sound using the boundary element method. *Applied Acoustics*, 65:1037–1056, 2003.

[12] D. L. Min, T. T. Kang, and S. S. Bo. Estimating the sound absorption coefficient of perforated wooden panels using artificial neural networks. *Applied Acoustics*, 70:31–40, 2009.

[13] M. Hodgson and K. Scherebnyj. Estimation of the absorption coefficients of the surfaces of classrooms. *Applied Acoustics*, 67:936–944, 2006.

[14] L. S. Wang, D. L. Lee, M. Y. Nie, and Z. W. Zheng. A study of the precision factors of large-scale object surface profile laser scanning measurement. *Journal of Material Processing Technology*, 129:584–587, 2002.

[15] F. Bosche and C. T. Hass. Automated retrieval for 3d cad model object in construction range images. *Automation in Construction*, 17:499–5123, 2008.

[16] P. Tang, D. Huber, B. Akicni, B. Lipman, and Lytle. Automatic reconstruction of as-built building information models from laser-scanned point clouds: A review of related techniques. *Automation in Construction*, 19:829–843, 2010.

[17] Ansi/asa s12.60-2010/part 1 american national standard acoustical performance criteria, design requirements, and guidelines for schools, part 1: Permanent schools.

[18] Iso 3382-2:2008(e): Acoustics-measurement of room acoustic parameters-part 2: Reverberation time in ordinary rooms.

[19] R. Tomiku, T. Otsuru, and Y. Takahashi. Finite element sound field analysis of diffuseness in reverberation time. *Journal of Asian Architecture and Building Engineering*, pages 33–39, 2000.

[20] S.R. Bistafa and J.S. Bradley. Prediction reverberation times in simulated classroom. *Journal of Acoustical Society of America*, 108:1721–1731, 2000.

[21] A. Billon, J. Picaut, and A. Sakout. Prediction of the reverberation times in high absorbent room using a modified-diffusion model. *Applied Acoustics*, pages 68–74, 2008.

[22] Z. Maekawa, J.H. Rindel, and P. Lord. *Environmental And Architectural Acoustics Second Edition*. Spon Press, 2011.

[23] C. H. Chen, L. F. Pau, and P. S. P. Wang. *The Handbook of Pattern Recognition and Computer Vision (2nd Edition)*. World Scientific Co., 1998.

[24] R. M. Haralick. Statistical and structural approaches to texture. *Proceeding of the IEEE*, 67:786–804, 1979.

[25] B. Tso and P. M. Mather. Classification of multisource remote sensing imagery using a genetic algorithm and markob random fields. *IEEE Transaction on Geoscience and Remote Sensing*, 37:1225–1260, 1999.

[26] F. Albregtsen. Statistical texture measures computed from gray level coocurrence matrices. Technical report, Department of Informatics, University of Oslo, 1995.

[27] E. S. Gadelmawla. A vision system for surface roughness characterization using the gray level co-occurrence matrix. *NDT & E. International*, 37:577–588, 2004.

[28] M. R. Chandraratne, S. Samarasinghe, D. Kulasiri, and R. Bickerstaffe. Pre-

diction of lamb tenderness using imahe surface texture features. *Journal of Food Engineering*, 77:492–499, 2006.

[29] D. S. Guru, Y. H. S. Kumar, and S. Manjunath. Textural features in flower classification. *Mathematical and Computer Modelling*, 54:1030–1036, 2011.

[30] C. E. Honetcutt and R. Plotnick. Image analysis techniques and gray-level co-occurrence matrices (glcm) for calculating bioturbation indices and characterizing biogenic sedimentary structures. *Computer & Geosciences*, 34:1461–1472, 2008.

[31] F. R. Renzetti and L. Zortea. Use of a gray level co-occurrence matrix to characterize duplex stainless steel phase microstructure. *Frattura ed Integrita' Strutturale*, 16:43–51, 2011.

[32] R. M. Haralick, K. Shanmugam, and I. Disntein. Textural features for image classificiation. *IEEE Transaction System, Man, and Cybernetics*, 3:610–621, 1973.

[33] S. Haykin. *Neural Networks and Learning Machines: 3rd Edition*. Prentice Hall, Upper Saddle River, New Jersey, 2009.

[34] D. Svozil, V. Pospíchal, and P. Kvasnička. Introduction to multi-layer feed-forward neural networks. *Chemometrics and Intelligent Laboratory System,*, 39:43–62, 1997.

[35] S. K. Lahiri and K. C. Ghanta. Development of an artificial neural network correlation for prediction of hold-up of slurry transport in pipeline. *Chemical Engineering Science*, 63:1467–1509, 2008.

[36] M. T. Haqan and M. Menhaj. Training feed forward forward with the marquardt algorithm. *IEEE Transactions Neural Networks*, 5:989–993, 1997.

[37] M. A. Hussain, M. Shafiur Rahman, and C. W. Ng. Prediction of pores formation (porosity) in food during drying: Generic model by use of hybrid

neural network. *Journal of Food Engineering*, 51:239–248, 2001.

[38] S. Shivastava and M. P. Singh. Performance evaluation of feed-forward neural networks with soft computing technique for hand written engligh alphabets. *Applied Soft Computing*, 11:1156–1182, 2011.

[39] E. Romero and R. Alque'zar. Comparing error minimized extreme learning machines and support vector squential feed-forward neural networks. *Neural Networks*, In Press, Corrected Proof, 2011.

[40] D .E. Rumelhart, G. E. Hinton, and R. J. Williams. Learning representations by back-propagation errors. *Nature*, 323:533–536, 1986.

[41] H. Demuth, M. Beale, and M. Hagan. *Neural Network Toolbox User's Guide*. The Mathworks. Inc, 2010.

[42] K. Levenberg. A method for the solution of certain non-linear problems in least squares. *The Quarterly of Applied Mathematics*, 2:164–168, 1944.

[43] D. Marquardt. An algorithm for least-squares estimation of nonlinear parameters. *SIAM Journal on Applied Mathematics*, 11(2):431–441, 1960.

[44] R. Singh, R.S. Bhoopal, and S. Kumar. Prediction of effective thermal conductivity of moist prorous materials using artificial neural network approach. *Building and Environment*, 46:2603–2608, 2011.

[45] A. Saengrung, A. Abtahi, and A. Zilouchian. Neural network model for a commercial pem fuel cell system. *Journal of Power Sources*, 172:749–759, 2007.

[46] M. Iwamoto and H. Chikatsu. Development of convenient 3d measurement using consumer grade digital camera: The 3dvision example. In *The International Archives of The Photogrammetric, Remote Sensing and Spatial Information Science. XXXVII, B6b Beijing, China*, 2008.

[47] C. Ordóñez, J. Martínez, P. Aría, and J. Armesto. A software program for

semi-automated measurement of building facades. *Measurement*, 43:1197–1206, 2010.

[48] Survey-from-photo taken from "www3.plala.or.jp/solidfromphoto/".

[49] C. Spa, A. Garriga, and J. Escolano. Impedance boundary conditions for pseudo-spectral time-domain methods in room acoustics. *Applied Acoustics*, 71:402–410, 2010.

[50] T. Okuzono, T. Otsuru, R. Tomiku, and N. Okamoto. Accuracy and efficiency of time domain finite element method for sound field analysis of room. In *Proceedings of Inter-Noise-2009. On CD ROM 2009*, 2009.

[51] J.E. Akin. *Finite element for Analysis and Design*. Academic Press Limited, 1997.

[52] N. M. Newmark. A method of computation for structural dynamics,. *Journal of the Engineering Mechanics Division*, 85:67–94, 1959.

[53] Matlab release 2010 taken from "http://www.mathworks.com/".

[54] *Image Processing Toolbox User's Guide*. The Mathworks. Inc, 2011.

[55] Z. Maekawa and P. Lord. *Environmental and Architectural Acoustics*. E & FN Spon, 1993.

[56] Y. Urano and H. Nakamura. *Architecture Environmental Engineering*. Moriko Co., 1996 (In Japanese).

[57] N. Ampazis and S. J. Perantonis. Levenberg-marquardt algorithm with adaptive momentum for the efficient training of feedforward networks. *Proceeding of the IEEE-INNS-ENNS International Joint Conference on Neural Networks*, 1:126–131, 2000.

[58] L. Prechelt. Automatic early stopping using cross validation: quantifying the citeria. *Neural Networks*, 11:761–767, 1998.

[59] M. H. Nguyen, H. A. Abbass, and R. I. McKay. Stopping criteria for ensemble of evolutionary artificial neural networks. *Applied Soft Computing*, 6:100–107, 2005.

[60] M. Shokrian, M. Sadrzadeh, and T. Mohammadi. c_3h_8 separation from ch_4 and h_2 using a synthesized pdms membrane: Experiment and neural network modeling. *Journal of Membrane Science*, 346:59–70, 2010.

[61] W. A. Young II, D. F. Millie, G. R. Wexkman, J. S. Anderson, D. M. Klarer, and G. L. Fahnenstied. Modeling net ecosystem metabolism with an artificial neural network and bayesian belief network. *Environmental Modelling & Software*, 26:1199–1210, 2011.

[62] S. S. Behzadi, C. Prakasvudhisarn, J. Klocker, P. Wolschann, and H. Viernstein. Comparison between two types of artificial neural networks used for validation of pharmaceutical processes. *Powder Technology*, 195:150–157, 2009.

[63] R. Tomiku, T. Otsuru, D. Azuma, and Y. Takahashi. Use of finite element method for comparison of sound field diffuseness in reverberation rooms with and without absorption material. *Acoustical Science and Technology*, pages 225–228, 2004.

[64] *Gid Use Manual Version 7. Digital Solution Inc. 2003.*

[65] J. Nannariello and F. Fricke. The prediction of reverberation time using neural networks analysis. *Applied Acoustics*, 58:305–325, 1999.

Part I.

Appendix I

PARAGRAH 1

I1=imread('DSC03542.JPG');

I2=imread('DSC03543.JPG');

I3=imread('DSC03544.JPG');

I4=imread('DSC03545.JPG');

I5=imread('DSC03546.JPG');

I6=imread('DSC03547.JPG');

I7=imread('DSC03548.JPG');

I8=imread('DSC03549.JPG');

I9=imread('DSC03550.JPG');

I10=imread('DSC03551.JPG');

.

.

.

PARAGRAH 2

K1 = rgb2gray(J1);

K2 = rgb2gray(J2);

K3 = rgb2gray(J3);

K4 = rgb2gray(J4);

K5 = rgb2gray(J5);

K6 = rgb2gray(J6);

K7 = rgb2gray(J7);

K8 = rgb2gray(J8);

K9 = rgb2gray(J9);

K10 = rgb2gray(J10);

.

.

.

PARAGRAH 3

offset=[0 1;-1 1;-1 0;-1 -1];

glcms1=graycomatrix(K1,'Offset',offset);

glcms2=graycomatrix(K2,'Offset',offset);

glcms3=graycomatrix(K3,'Offset',offset);

glcms4=graycomatrix(K4,'Offset',offset);

glcms5=graycomatrix(K5,'Offset',offset);

glcms6=graycomatrix(K6,'Offset',offset);

glcms7=graycomatrix(K7,'Offset',offset);

glcms8=graycomatrix(K8,'Offset',offset);

glcms9=graycomatrix(K9,'Offset',offset);

glcms10=graycomatrix(K10,'Offset',offset);

.

.

.

PARAGRAH 4

DSC03542=graycoprops(glcms1,'Contrast Correlation Energy Homogeneity');

DSC03543=graycoprops(glcms2,'Contrast Correlation Energy Homogeneity');

DSC03544=graycoprops(glcms3,'Contrast Correlation Energy Homogeneity');

DSC03545=graycoprops(glcms4,'Contrast Correlation Energy Homogeneity');

DSC03546=graycoprops(glcms5,'Contrast Correlation Energy Homogeneity');

DSC03547=graycoprops(glcms5,'Contrast Correlation Energy Homogeneity');

DSC03548=graycoprops(glcms7,'Contrast Correlation Energy Homogeneity');

DSC03549=graycoprops(glcms8,'Contrast Correlation Energy Homogeneity');

DSC03550=graycoprops(glcms9,'Contrast Correlation Energy Homogeneity');

DSC03551=graycoprops(glcms1,'Contrast Correlation Energy Homogeneity');

.

.

.

Part II.

Appendix II

PARAGRAH 1

```
load trainnorm2.txt
[G ,H]= size(trainnorm2);
rawdata=trainnorm2(randperm(G),1:5); % Randomize
[R Q]=size(rawdata);
P1 = rawdata(:,1); % contrast
P1 = P1';
P2 = rawdata(:,2); % correlation
P2 = P2';
P3 = rawdata(:,3); % ASM
P3=P3';
P4 = rawdata(:,4); % homogeinity
P4 = P4';

T1 = rawdata(:,5); % alpha type of material
T1 = T1';

for i=1:R
    data(1,i) = P1(i);
    data(2,i) = P2(i);
    data(3,i) = P3(i);
    data(4,i) = P4(i);
    data(5,i) = T1(i);
end
```

PARAGRAH 2

```
%NORMALIZE (0.1,0.9)

[N , M] = size(data);
for i = 1:N
```

```
    max(i) = data(i,1);
    min(i) = data(i,1);
    for j = 1:M
        if data(i,j)>max(i)
        max(i)=data(i,j);
        end
        if data(i,j)<min(i)
        min(i)=data(i,j);
        end
    end
    rawdata1(i,:) = 0.1+[0.8*(data(i,:)-min(i))/(max(i)-min(i))]; % normalize (0.1,0.9)
end


  randdata=rawdata1;
  P=randdata(1:4,:);
  T=randdata(5,:);

  iitr1=1:100;
  iitv1=101:134;
  unseen=135:168;

  trP1 = P(:,iitr1); % Input for Train
  v.P = P(:,iitv1); % Input for Validate
  t.P = P(:,unseen); % Input for Testing

  trT1 = T(:,iitr1); % Output for Train
  v.T = T(1,iitv1); % Output for Validate
  t.T = T(:,unseen); % Output for Testing
```

PARAGRAH 3

```
s1=7;% number of hidden node
    net=newff(minmax(trP1),[s1 1],{'tansig','purelin'},'trainlm');

    net.performFcn = 'mse';
    net=init(net);
    tic,[net,tr]=train(net,trP1,trT1,[],[],v,t);toc;
```

PARAGRAH 4

```
% CHECK PERFORMANCE

    an1=sim(net,trP1);
    e1=trT1-an1;
    an2=sim(net,v.P);
    e2=v.T-an2;
    an3=sim(net,t.P);
    e3=t.T-an3;
    perf_train=mse(e1)
    per_validate=mse(e2)
    per_test=mse(e3)

    figure [m1,b1,r1]=postreg(trT1,an1);
    figure [m1,b1,r1]=postreg(v.T,an2);
    figure [m1,b1,r1]=postreg(t.T,an3);
```

Part III.

Appendix III

no of dimension	measured values	System 2 values	difference values
1	6.09	5.8902	0.19985
2	3.02	2.9829	0.03711
3	5.749	5.5796	0.16943
4	0.291	0.28851	0.0024944
5	0.36	0.31931	0.04069
6	2.716	2.6154	0.10061
7	2.214	2.1376	0.076364
8	2.01	1.9331	0.076874
9	1.2	1.1808	0.019155
10	4.504	4.4054	0.098609
11	1.2	1.2017	-0.0016729
12	4.504	4.4134	0.090565
13	5.9	5.7416	0.15845
14	5.9	5.7498	0.15022
15	0.065	0.060708	0.0042918
16	0.065	0.062569	0.002431
17	1.69	1.589	0.10102
18	1.18	1.1634	0.016647
19	1.18	1.1752	0.0047732
20	0.118	0.11189	0.0061095
21	0.069	0.062915	0.0060853
22	0.118	0.11249	0.0055139
23	0.069	0.061351	0.0076491
24	1.258	1.1733	0.084702
25	0.244	0.20449	0.039509
26	1.258	1.1918	0.066244
27	0.244	0.19639	0.047609

no of dimension	measured values	System 2 values	difference values
28	0.71	0.67265	0.037348
29	0.512	0.44371	0.068288
30	0.71	0.66175	0.048253
31	0.512	0.46059	0.051413
32	0.56	0.56505	-0.0050492
33	0.56	0.67017	-0.11017
34	0.56	0.58252	-0.022523
35	0.56	0.68848	-0.12848
36	7.083	6.7859	0.2971
37	3.02	2.8231	0.19688
38	7.083	6.7779	0.30513
39	3.02	2.7716	0.24837
40	2	1.8903	0.10972
41	2.214	2.1217	0.092284
42	2	1.8985	0.10149
43	2.214	2.0545	0.15946
44	2.602	2.5245	0.077509
45	2.214	2.098	0.11597
46	2.602	2.5139	0.088078
47	2.214	2.1349	0.079083
48	0.555	0.56334	-0.0083388
49	0.445	0.43485	0.010148
50	0.555	0.5667	-0.011695
51	0.445	0.43526	0.0097406
52	0.458	0.45355	0.0044537
53	0.608	0.59288	0.015117
54	0.458	0.45617	0.0018326
55	0.608	0.59116	0.01684

no of dimension	measured values	System 2 values	difference values
56	0.065	0.052884	0.012116
57	0.118	0.10416	0.013841
58	0.069	0.064757	0.0042435
59	0.118	0.10532	0.012676
60	0.069	0.056677	0.012323
61	0.244	0.22947	0.014533
62	1.258	1.3172	-0.05922
63	0.244	0.21683	0.027175
64	1.258	1.2849	-0.026853
65	0.71	0.75856	-0.048561
66	0.512	0.52244	-0.010436
67	0.71	0.78608	-0.076082
68	0.512	0.51386	-0.0018621
69	7.083	6.8843	0.19874
70	2.716	2.5372	0.17877
71	0.36	0.27299	0.087009
72	0.291	0.28474	0.0062649
73	7.083	7.0724	0.010631
74	0.291	0.28123	0.0097696
75	0.36	0.27171	0.088294
76	2.716	2.5113	0.20466
77	7.083	7.0911	-0.0081053
78	7.083	6.8705	0.21249
79	6.206	6.096	0.10996
80	1.69	1.5918	0.098218
81	6.206	6.0624	0.14356
82	1.69	1.5826	0.10743

no of dimension	measured values	System 2 values	difference values
83	1.562	1.5588	0.0031977
84	1.604	1.5317	0.072345
85	1.562	1.5534	0.0085843
86	1.604	1.5333	0.07072
87	1.448	1.4107	0.037266
88	1.604	1.5117	0.092269
89	1.448	1.3994	0.04856
90	1.604	1.5296	0.074402
91	0.065	0.056385	0.0086155
92	0.065	0.058463	0.0065372
93	1.258	1.3627	-0.10472
94	0.244	0.18516	0.058842
95	1.258	1.3268	-0.068828
96	0.244	0.22598	0.018022
97	1.258	1.361	-0.10301
98	0.244	0.21359	0.030406
99	1.258	1.3233	-0.065256
100	0.244	0.19985	0.044155